THE INFLUENCE OF CONDUCTING FLAPS ON THE REFLECTION COEFFICIENT OF A PARALLEL-PLATE WAVEGUIDE ILLUMINATING A CONDUCTING SHEET

L.L. Tsai and R.C. Rudduck

The Ohio State University

ElectroScience Laboratory

(formerly Antenna Laboratory)

Department of Electrical Engineering

Columbus, Ohio 43212

TECHNICAL REPORT 2143-5

9 April 1968

Grant Number NGR-36-008-048

National Aeronautics and Space Administration

Office of Grants and Research Contracts

Washington, D.C. 20546

NOTICES

When Government drawings, specifications, or other data are used for any purpose other than in connection with a definitely related Government procurement operation, the United States Government thereby incurs no responsibility nor any obligation whatsoever, and the fact that the Government may have formulated, furnished, or in any way supplied the said drawings, specifications, or other data, is not to be regarded by implication or otherwise as in any manner licensing the holder or any other person or corporation, or conveying any rights or permission to manufacture, use, or sell any patented invention that may in any way be related thereto.

The Government has the right to reproduce, use, and distribute this report for governmental purposes in accordance with the contract under which the report was produced. To protect the proprietary interests of the contractor and to avoid jeopardy of its obligations to the Government, the report may not be released for non-governmental use such as might constitute general publication without the express prior consent of The Ohio State University Research Foundation.

REPORT 2143-5

REPORT

by

The Ohio State University ElectroScience Laboratory
(Formerly The Antenna Laboratory)
Columbus, Ohio 43212

Sponsor	National Aeronautics and Space Administration Office of Grants and Research Contracts Washington, D.C. 20546
Grant No.	NGR-36-008-048
Investigation of	Theoretical and Experimental Studies of Antennas for Reflectometer Application
Subject of Report	The Influence of Conducting Flaps on the Reflection Coefficient of a Parallel-Plate Waveguide Illuminating a Conducting Sheet
Submitted by	L.L. Tsai and R.C. Rudduck ElectroScience Laboratory Department of Electrical Engineering
Date	9 April 1968

ABSTRACT

The influence of conducting flaps on the reflection coefficient of a ground-plane-mounted TE_{01} mode parallel-plate waveguide illuminating a reflecting sheet is analyzed. The backscatter from the guide is determined by use of wedge diffraction and surface integration techniques. The reflection coefficient of the guide is then obtained through an iterative procedure that describes the multiple interactions between the guide and reflector as bouncing cylindrical waves. The optimum flap length produces a significant reduction in the backscatter from the guide and consequently a significant reduction in the oscillations of the reflection coefficient.

TABLE OF CONTENTS

THE INFLUENCE OF CONDUCTING FLAPS ON THE REFLECTION COEFFICIENT OF A PARALLEL-PLATE WAVEGUIDE ILLUMINATING A CONDUCTING SHEET

I. INTRODUCTION

Recent advances in space exploration has given impetus to the need for better understanding of spacecraft antenna problems. An important phenomenon is communications blackout encountered during reentry due to plasma formation. In order to overcome this problem, a knowledge of the characteristics of the plasma formed around the spacecraft is necessary. A widely used technique for plasma diagnostics is a flight measurement of antenna impedances or reflection coefficients. Improved designs are being sought for reflectometer antennas useful for this purpose. One approach being taken to gain insight into the behavior of reflectometer antennas is to analyze the aperture reflection coefficient of a waveguide illuminating a conducting sheet which approximates a cutoff plasma. The interactions between the conducting sheet and the ground-plane-mounted waveguide are similar to those which occur between a cutoff plasma and the vehicle skin around the reflectometer antenna. Consequently this type of analysis gives a measure of the performance of flush mounted reflectometer antennas.

A. Statement of the Problem

The problem being treated in this report is the analysis of the reflection coefficient of a ground-plane-mounted TE_{01} mode parallel-plate waveguide with flaps attached at the aperture and illuminating a conducting sheet. The geometry of the problem is as shown in Fig. 1.

A similar problem which has been previously treated[1,2] is the TEM mode ground-plane-mounted guide (without flaps) illuminating a conducting sheet. By using the wedge diffraction method the reflection from the conducting sheet was given in terms of successive contributions or bounces that describe the interacting waves between the waveguide and the reflector. Each of these bounce waves was subsequently resolved into component cylindrical waves. The reflection coefficient was then obtained by summing these iterative contributions. For the TEM guide without flaps, the reflection coefficients when plotted as a function of d, the reflector spacing, exhibited strong oscillatory behavior. In fact, for values of d equal to an integral multiple of $\lambda/2$, complete reflection, or a unity reflection coefficient, was observed.

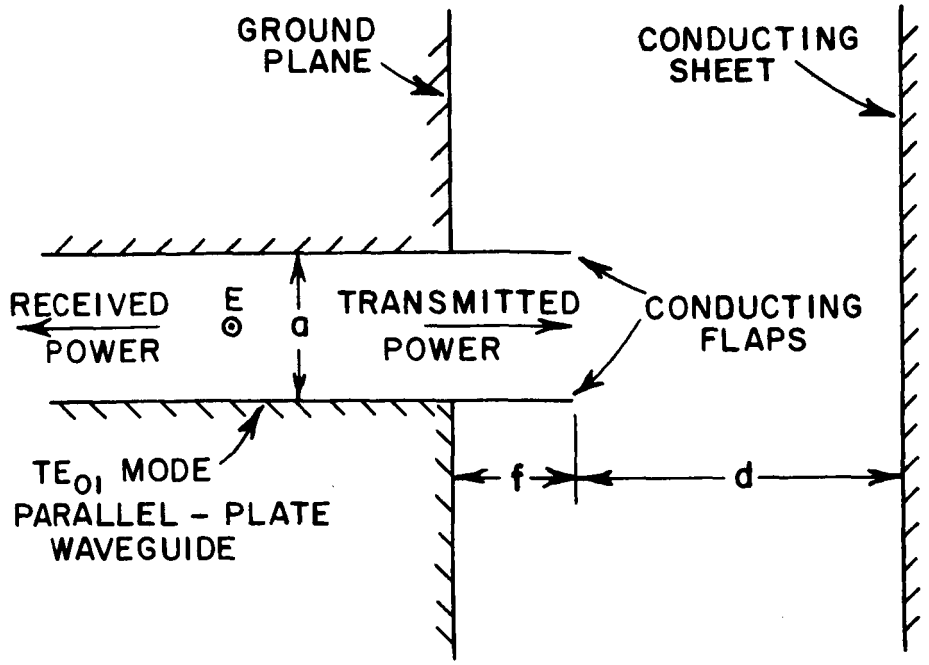

Fig. 1. TE_{01} mode parallel-plate waveguide with flaps illuminating a conducting sheet.

In order to accurately determine the distance d of a perfectly reflecting surface from an antenna in a ground plane, however, it is desirable to have the reflection magnitude from the antenna be a monotone function of d. The ground plane mounted TEM guide studied in Ref. 2 is therefore unsuitable for reflectometer applications without further modifications.

The problem considered in this report is motivated by the work of R. Lentz[3] where he experimentally observed that the reflected power received by an absorber-backed pyramidal horn illuminating a reflecting sheet may be made a monotone function of the distance to the reflector by the attachment of conducting flaps to the E-plane edges of the horn. However, the important question remaining unanswered is: can a ground plane mounted aperture antenna achieve this monotone reception, since the ground plane is the primary scatterer? For this case significant multiple interactions can occur between the ground plane and reflector so as to yield oscillatory results. The purpose of this investigation is then to examine the effect of conducting flaps in reducing these multiple interactions.

The method of solution for the flap guide problem is outlined below. First, the backscatter of the guide structure with flaps is determined

for plane wave incidence by applications of wedge diffraction and surface integration techniques. The scattered field is then observed on a plane at a constant distance away from the guide aperture for different flap lengths (f). The optimum flap length is that which yields the deepest null in the scattered field since this means the lowest return from the guide structure and hence lowest multiple interactions between the guide and reflector. Secondly, the scattered field is resolved by superposition to be the sum of two equivalent line source fields plus the reflected geometrical optics field. Finally, the reflection coefficient is analyzed by a multiple bounce procedure similar to that employed in Ref. 2.

B. Background

Following the method in Refs. 4 and 5, the incident field in a TE_{01} mode parallel plate waveguide may be expressed in terms of plane waves (as shown in Fig. 2) where the angle of propagation is given by

$$A_o = \sin^{-1} \frac{\lambda}{2a} \quad . \tag{1}$$

The incident modal power flow is

$$P_o = 2a\, Y_o \cos A_o \tag{2}$$

where

$$Y_o = \sqrt{\epsilon_o / \mu_o} \quad ,$$

and the associated modal voltage is

$$V_o = \sqrt{2a \frac{Y_o}{Y_g} \cos A_o} \tag{3}$$

where Y_g is the guide admittance for the TE_{01} mode. For this polarization the relationship between the electric field E, ray R, diffraction coefficient D, and modal voltage V is given by

$$E = R \frac{e^{-j(kr + \pi/4)}}{\sqrt{2\pi kr}} = D \frac{e^{-jkr}}{\sqrt{r}} = V \frac{e^{-jkr + \pi/4}}{\sqrt{2\pi r}} \tag{4}$$

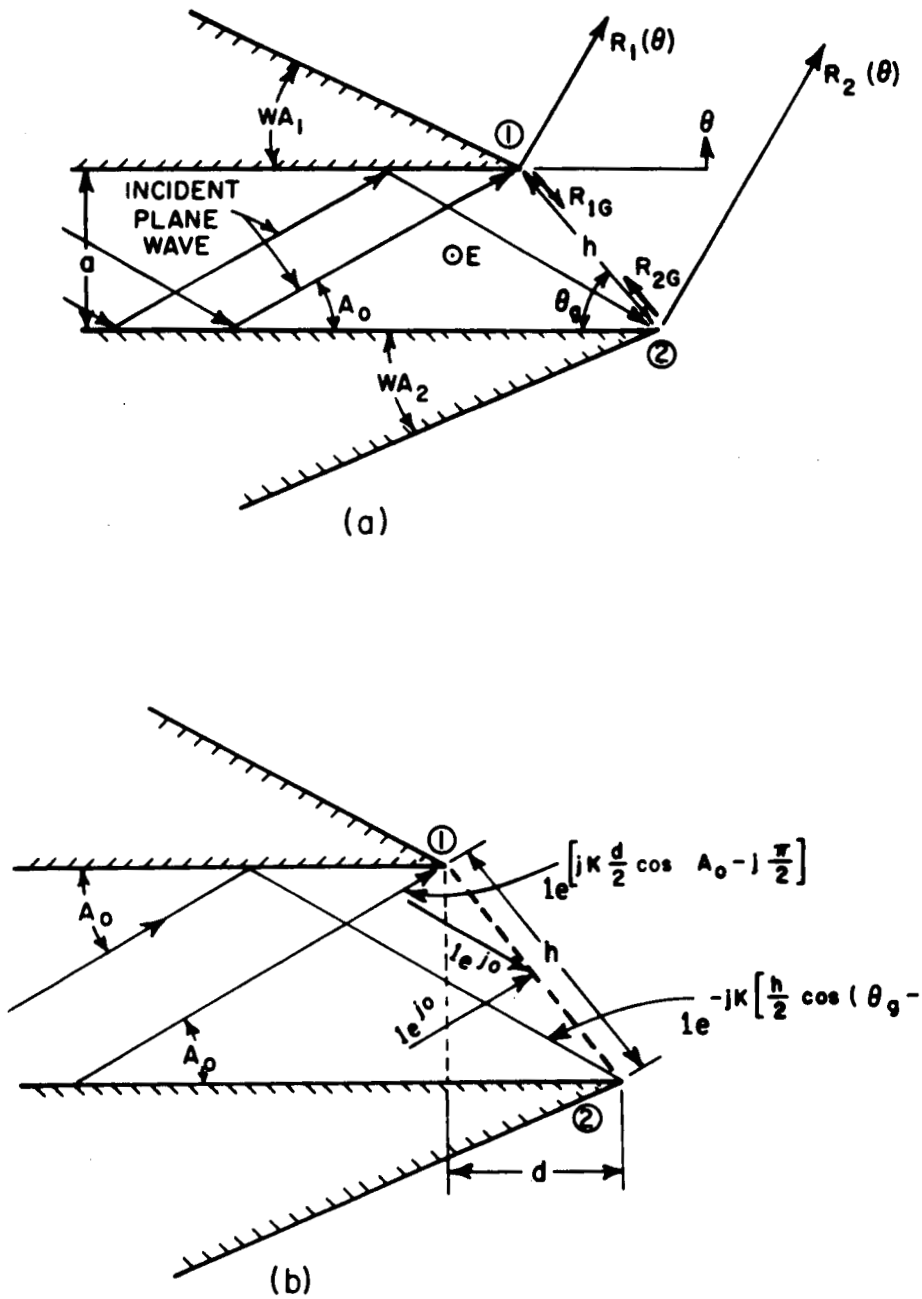

Fig. 2. TE_{01} mode in a parallel-plate waveguide.

The diffraction at the aperture of the parallel-plate waveguide may be treated as in Ref. 4 by summing the single and double diffraction contributions. The guide structure in this analysis may be approximated by a symmetric half-plane guide when considering radiation in the on-axis region. The singly diffracted rays from edges 1 and 2 are thus given respectively by

$$(5) \qquad R_1^{(1)}(\theta) = \frac{1}{n_1} \sin\frac{\pi}{n_1} \left[\frac{1}{\cos\frac{\pi}{n_1} - \cos\frac{\pi+\theta-A_o}{n_1}} - \frac{1}{\cos\frac{\pi}{n_1} - \cos\frac{\pi+\theta+A_o}{n_1}} \right] e^{-j\pi/2} ,$$

and

$$(6) \qquad R_2^{(1)}(\theta) = \frac{1}{n_2} \sin\frac{\pi}{n_2} \, e^{-j\pi/2} \times \left[\frac{1}{\cos\frac{\pi}{n_2} - \cos\frac{\pi-\theta-A_o}{n_2}} - \frac{1}{\cos\frac{\pi}{n_2} - \cos\frac{\pi-\theta+A_o}{n_2}} \right]$$

where $n_1 = n_2 = 2.0$.

The ray from edge 1 (or 2) which illuminates edge 2 (or 1) is given by

$$(7) \qquad R_1 G^{(1)} = R_2 G^{(1)} = R_1^{(1)}(-90°) = R_2^{(1)}(90°) .$$

The doubly diffracted rays from the two edges are given by

$$(8) \qquad R_1^{(2)}(\theta) = R_2 G^{(1)} \left[V_B(a, 90° + \theta, n_1) - V_B(a, 270° + \theta, n_1) \right] ,$$

and

$$R_2^{(2)}(\theta) = R_1 G^{(1)}[V_B(a, 90° - \theta, n_2) - V_B(a, 270° - \theta, n_2)] ,$$

where $V_B(r, \phi, n)$ is the wedge diffraction function employed in previous analyses. Calculations have shown[6] that the field radiated by the guide near the on-axis region may be approximated by a line source field given by

$$(9) \qquad E_T(\theta=0, r) = R_T(\theta=0) \frac{e^{-j(kr+\pi/4)}}{\sqrt{2\pi kr}} = D_T(\theta=0) \frac{e^{-jkr}}{\sqrt{r}}$$

where

$$R_T(\theta=0) = R_1^{(1)}(\theta=0) + R_2^{(1)}(\theta=0) + R_1^{(2)}(\theta=0) + R_2^{(2)}(\theta=0) .$$

The equivalent line source with modal voltage V_1 which approximates the guide radiation is then given by

$$(10) \qquad E_T(0, r) = V_1 \frac{e^{-j(kr-\pi/4)}}{\sqrt{2\pi r}} .$$

A primary result used in this analysis is the response of the TE_{01} mode parallel-plate waveguide to an incident cylindrical wave. This is given by the line source to waveguide coupling relationship presented in Ref. 5 as

$$(11) \qquad V = \sqrt{\frac{Y_o}{Y_g}} \frac{\sqrt{\lambda}\ e^{-j\pi/4}}{\sqrt{2a \cos A_o}} D_T(\theta)\ E^i ,$$

where V is the modal voltage induced in the guide, E^i is the incident field at the guide aperture center, and $D_T(\theta)$ is the diffraction coefficient of the guide given through Eq. (9). Rewriting this relationship in a form useful for computing the reflection coefficient Γ, we find

$$(12) \qquad \Gamma = \frac{V}{V_o} = C\, V^i \frac{e^{-jkr}}{\sqrt{r}} ,$$

where V^i is the modal voltage of the line source generating the incident field E^i given by

$$E^i = V^i \frac{e^{-jkr + j\pi/4}}{\sqrt{2\pi r}} \quad , \tag{13}$$

and the constant C is given in terms of the on-axis ray $R_T(\theta = 0)$ as

$$C = \frac{\sqrt{\lambda}}{2a \cos A_o} \quad \frac{R_T(\theta=0)\, e^{-j\pi/4}}{2\pi\sqrt{k}} \quad . \tag{14}$$

II. BACKSCATTERING OF GUIDE WITH FLAPS

In this section the backscattering properties of the guide structure shown in Fig. 1 are investigated as a function of flap length. Assuming a unit amplitude plane wave incident on the guide as shown in Fig. 3, the scattered field may be analyzed by a combination of wedge diffraction and surface integration techniques. The scattered field is then observed on a plane normal to the guide axis and located at a distance d' away from the guide aperture. The flap length which gives the deepest null in the total scattered field may then be considered optimal for minimizing multiple interactions between the guide and the reflector.

The scattered field for this problem may be thought of as being composed of the following components: (1) direct diffraction contributions or the diffracted rays from the flap edges which are not influenced by the presence of the ground plane; (2) reflected diffraction contributions or the diffracted rays from the flaps which reflect off the ground plane and contribute to the total scattered field, and (3) reflected geometrical optics contributions from the ground plane. Detailed analyses of these components are given in the following sections.

A. Direct Diffraction Contributions

The analysis of the direct diffraction contributions from the flap edges is analogous to that employed in previous problems.[1,7,8] These contributions may be obtained by simply summing the single and double diffraction contributions from the flap edges as shown in Fig. 4.

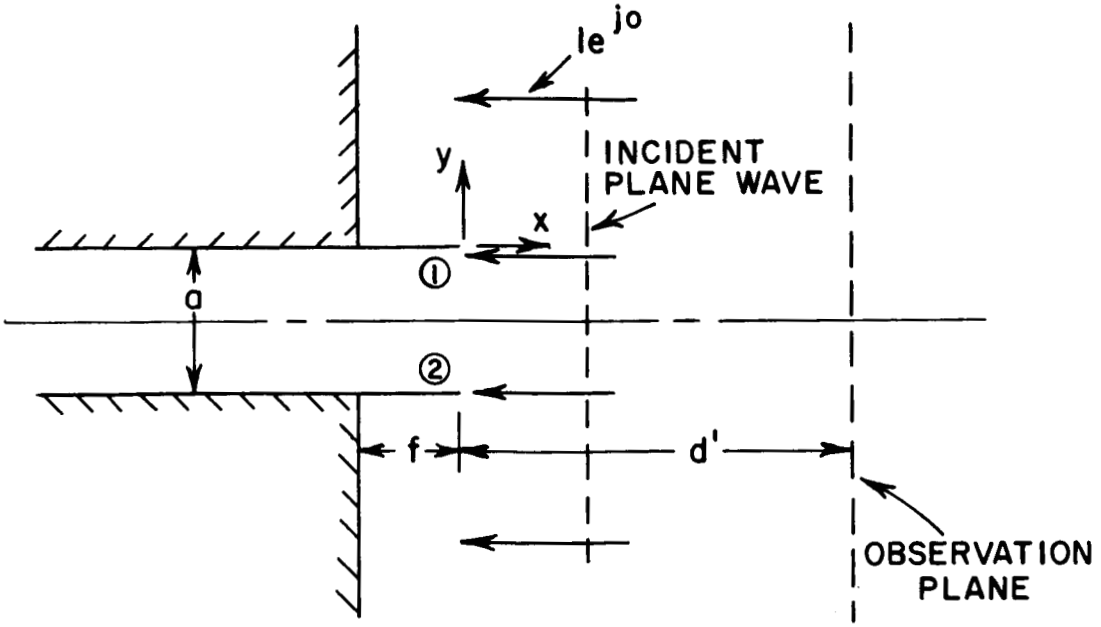

Fig. 3. Unity amplitude plane wave normally incident on the guide.

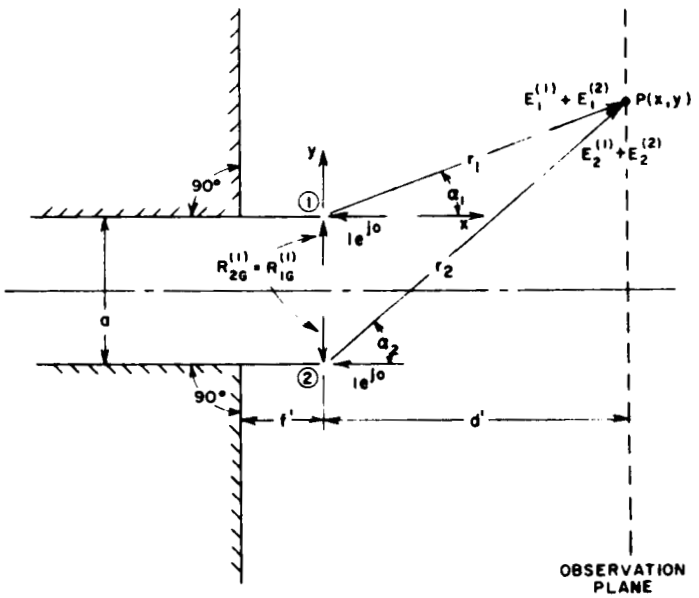

Fig. 4. Direct diffraction contributions to the scattered field from the flap edges.

The singly diffracted field at the observation point P(x, y) from edges 1 and 2 are given, respectively, by

$$E_1^{(1)} = V_B(r_1, \alpha_1, 2.0) - V_B(r_1, 2\pi + \alpha_1, 2.0) \tag{15}$$

where

$$r_1 = \sqrt{d'^2 + y^2}$$

and

$$\alpha_1 = \tan^{-1}(y/d')$$

and

$$E_2^{(1)} = V_B(r_2, -\alpha_2, 2.0) - V_B(r_2, 2\pi - \alpha_2, 2.0) \tag{16}$$

where

$$r_2 = \sqrt{d'^2 + (y + a)^2}$$

and

$$\alpha_2 = \tan^{-1}\left(\frac{y+a}{d'}\right) \quad .$$

The single diffraction rays which originate at one edge and illuminate the opposite edge are given by

$$R_1G^{(1)} = R_2G^{(1)} = \frac{1}{n}\sin\frac{\pi}{n}\left[\frac{1}{\cos\frac{\pi}{n} - \cos\frac{90°}{n}} - \frac{1}{\cos\frac{\pi}{n} - \cos\frac{270°}{n}}\right] \tag{17}$$

$$= -\sqrt{2} \text{ for } n = 2.0$$

Hence the doubly diffracted field from edges 1 and 2 are given, respectively, by

$$(18)\qquad E_1^{(2)} = R_2 G^{(1)} \frac{e^{-j\pi/4}}{\sqrt{2\pi k}} \frac{e^{jk\left[\frac{ar_1}{r_1+a} - (r_1+a)\right]}}{\sqrt{r_1+a}}$$

$$\times \left[V_B\left(\frac{r_1 a}{r_1+a}, 90^\circ + \alpha_1, 2.0\right) - V_B\left(\frac{r_1 a}{r_1+a}, 270^\circ + \alpha_1, 2.0\right)\right]$$

and

$$(19)\qquad E_2^{(2)} = R_1 G^{(1)} \frac{e^{-j\pi/4}}{\sqrt{2\pi k}} \frac{e^{jk\left[\frac{r_2 a}{r_2+a} - (r_2+a)\right]}}{\sqrt{r_2+a}}$$

$$\times \left[V_B\left(\frac{r_2 a}{r_2+a}, 90^\circ - \alpha_2, 2.0\right) - V_B\left(\frac{r_2 a}{r_2+a}, 270^\circ - \alpha_2, 2.0\right)\right] .$$

The total direct diffraction contribution to the scattered field may then be expressed as

$$(20)\qquad E_D = E_1^{(1)} + E_2^{(1)} + E_1^{(2)} + E_2^{(2)} .$$

B. Reflected Diffraction Contributions

The diffracted rays from the edges of the flaps which reflect off the ground plane and thus contribute to the total scattered field may be analyzed to a first order approximation by the same ray tracing technique employed in the previous section. If this method were applied the geometry and diffraction components involved would be as shown in Fig. 5 where E_{RD} represents the diffracted wave which emanates from edge 1, is reflected by the ground plane, and contributes to the scattered field at P(x, y). A similar process, of course, results from edge 2 for $y < -a$. Preliminary calculations have shown that this technique would be adequate if one were interested only in finding the scattered field for $|y| >> 0$. However, for the regions of interest in the problem of this report further considerations must be given.

The reflected diffraction wave, E_{RD}, can be seen in Fig. 5 to actually reilluminate edge 1 as $\beta \rightarrow 0$. The subsequent diffracted wave

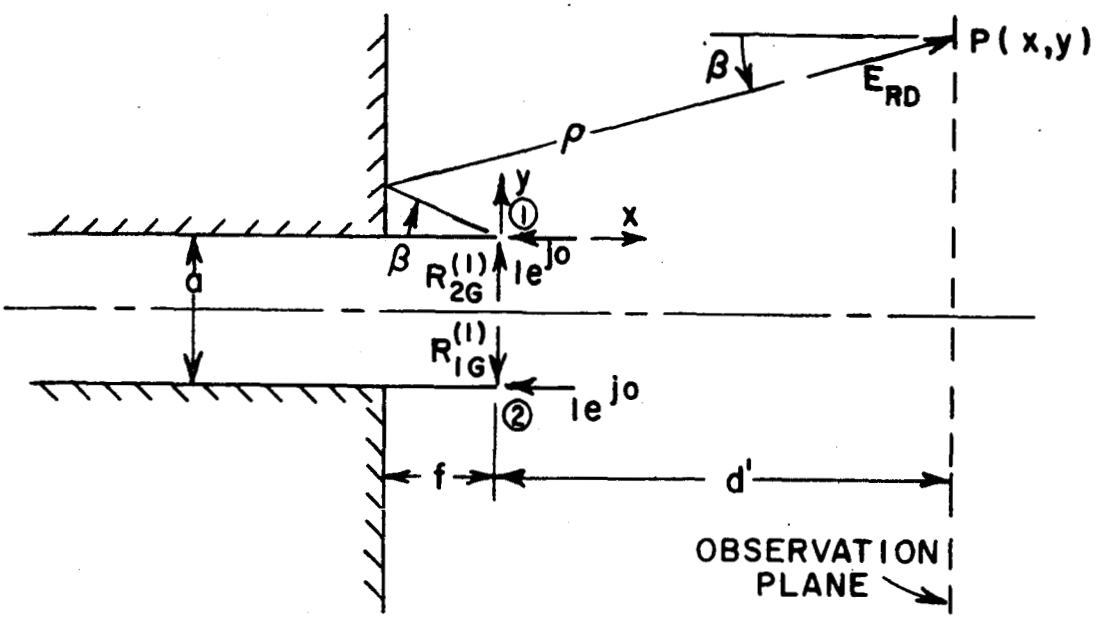

Fig. 5. Ray tracing technique for finding the reflected diffraction contributions from the flaps.

which results cannot be adequately described by conventional wedge diffraction techniques, which inherently assumes cylindrical wave incidence, because the magnitude of E_{RD} rapidly approaches a sharp peak with a steep slope near the surface of the flap. Consequently, a surface integration technique is applied to include the effects of this nonuniform wave.

Basically, the surface integration technique treats multiple interactions which occur in diffraction problems by integrating the diffracted fields of an interaction wave of a specific order over a surface, to obtain what corresponds to the subsequent order wedge-diffracted wave. This method has been successfully used in Refs. 9 and 10 and have been shown to provide higher accuracies than the wedge diffraction method while precluding the limitations of nonuniform wave interactions.

Formulating the analysis of the reflected diffraction components by the surface integration technique, the pertinent parameters are as shown in Fig. 6. The surface of integration is chosen to be at the guide aperture plane. First, the reflected diffraction fields, E'_{RD}, on the surface of integration will be determined. Then the reflected diffraction

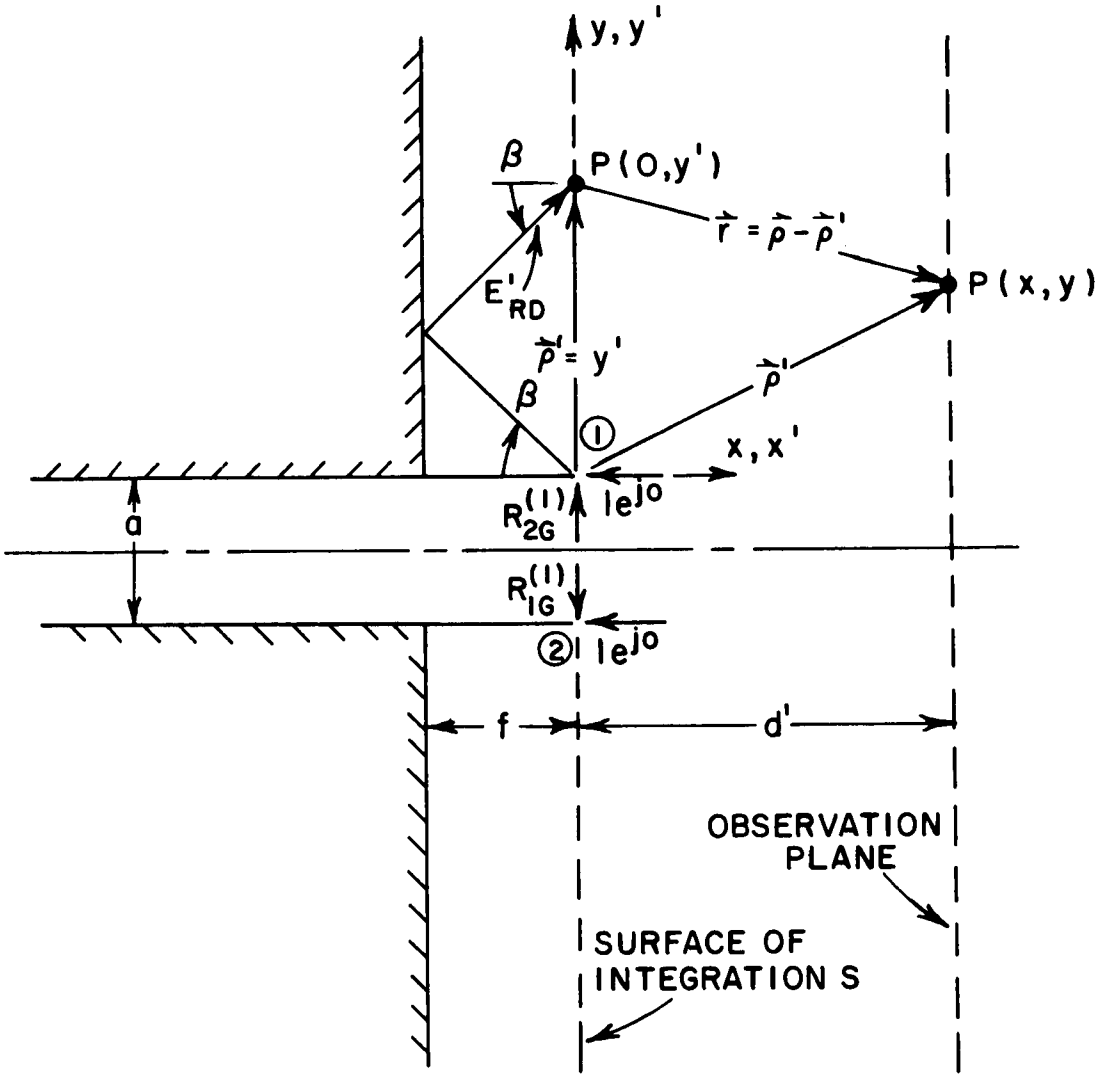

Fig. 6. Applications of surface integration techniques to analyze the reflected diffraction contributions from the flaps.

contributions, E_{RD}, at the observation plane will be determined using Green's Second Identity for planar surfaces[11] given by

$$(21) \qquad E_{RD}(x, y) = 2 \int_{-\infty}^{\infty} E'_{RD}(0, y') \left. \frac{\partial G_o}{\partial x'} \right|_{x'=0} dy' ,$$

where

$$G_o(kr) = - \frac{j}{4} H_o^{(2)}(kr)$$

with

$$\vec{r} = \vec{p} - \vec{p}' \quad .$$

Noting that $r = \sqrt{(x-x')^2 + (y-y')^2}$, Eq. (21) may be simplified by the following relationship

$$(22) \qquad \left. \frac{\partial G_o(kr)}{\partial x'} \right|_{x'=0} = \left[\frac{\partial G_o(kr)}{\partial (kr)} \frac{\partial (kr)}{\partial x'} \right]_{x'=0}$$

$$= \frac{1}{4j} H_1^{(2)}(kr) \frac{kx}{r} \quad ,$$

where $H_1^{(2)}(kr)$ is the Hankel function of the second kind of first order.

The reflected diffraction field on the surface of integration S is given by summing the single and double diffraction contributions. For $y' > 0$ only edge 1 will contribute and for $y' < -a$ only edge 2 will contribute while for $0 > y' > -a$ the reflected diffraction field is zero on S. It may be recognized that due to the symmetry about the guide axis, identical field distributions exist for $y' > 0$ and for $y' < -a$, thus only the upper half of S needs to be treated. The singly diffracted field from edge 1 is thus given by

$$(23) \qquad E_1^{(1)'}(y') = - [V_B(\rho', \beta - \pi) - V_B(\rho', \beta + \pi)] ,$$

where the minus sign results from the reflection from the ground plane and the geometrical quantities are

$$\beta = \tan^{-1}\left(\frac{y'}{2f}\right) \quad ,$$

and

$$\rho' = \sqrt{y'^2 + (2f)^2} \quad .$$

The doubly diffracted field from edge 1 is similarly given by

$$(24) \qquad E_1^{(2)'}(y') = -R_1 G^{(1)} \frac{e^{-j\pi/4}}{\sqrt{2\pi k}} \frac{e^{jk\left[\frac{a\rho'}{\rho'+a} - (\rho'+a)\right]}}{\sqrt{\rho'+a}}$$

$$\times \left[V_B\left(\frac{\rho' a}{\rho'+a}, 270° - \beta, 2.0\right) - V_B\left(\frac{\rho' a}{\rho'+a}, 450° - \beta, 2.0\right)\right] \quad .$$

The total reflected diffraction field on S for $y' > 0$ is thus given by

$$(25) \qquad E'_{RD}(y') = E_1^{(1)'}(y') + E_1^{(2)'}(y') \quad .$$

The symmetry property of the field on S will now be invoked to simplify Eq. (21). Let

$$(26) \qquad E_{RD}(x, y) = E_I(x, y) + E_{II}(x, y) \ ,$$

where

$E_I(x, y)$ = field at $P(x, y)$ by integration over the upper half of S

$$= 2 \int_0^\infty E_{RT}'(0, y') \left.\frac{\partial G_o}{\partial x'}\right|_{x'=0} dy' \quad ,$$

and

$E_{II}(x, y)$ = field at $P(x, y)$ by integration over the lower half of S

$$= 2 \int_{-\infty}^{-a} E'_{RT}(0, y') \left. \frac{\partial G_o}{\partial x'} \right|_{x'=0} dy' \quad .$$

Then, by symmetry,

$$E_{II}(x, y) = E_I(x, -y-a) \quad . \tag{27}$$

Rewriting Eq. (21), the total reflected diffraction contribution to the scattered field at $P(x, y)$ is thus given by

$$E_{RD}(x, y) = E_I(x, y) + E_I(x, -y-a) \tag{28}$$

$$= 2 \int_0^{\infty} E'_{RD}(0, y') \left[\left. \frac{\partial G_o}{\partial x'} \right|_{\substack{x'=0 \\ (x, y)}} + \left. \frac{\partial G_o}{\partial x'} \right|_{\substack{x'=0 \\ (x, -y-a)}} \right] dy'$$

with the integrand given through Eqs. (22) and (25).

It may be noted in passing that the direct diffraction contributions obtained by ray techniques in Section A may also be analyzed by surface integration techniques. However, when interaction waves are uniform to a good approximation, this more tedious technique is not necessary and, in fact, can be shown to yield values directly corresponding to the ray technique.[9]

C. Reflected Geometrical Optics Contributions

Analogous to the reflected diffraction contribution in the previous section, the reflected geometrical optics component may be seen to also reilluminate the flap edges. Conventional wedge diffraction theory again cannot be applied directly since this component is actually discontinuous along the surface of the flap. Surface integration techniques together with superposition is therefore applied to analyze this component.

It may be noted here that both the reflected geometrical optics field, E_{RG}, and the reflected diffracted field, E_{RD}, are discontinuous at the surface of the flaps. But in order to satisfy the boundary conditions for this polarization their sum, i.e., $E_{RD} + E_{RG}$, must be continuous and approach zero along the flap surface.

The geometry involved for E_{RG} is the same as that in Fig. 6 with the surface of integration S at the aperture plane. The reflected geometrical optics field on S is given by

$$(29) \qquad E'_{RG}(y') = \begin{cases} -e^{-jk(2f)} & \text{for } y' > 0 \text{ or } y' < -a, \\ 0 & \text{for } 0 \geq y' \geq -a \end{cases}$$

where the minus sign arises from the reflection by the ground plane. By superposition E_{RG} may be resolved as shown in Fig. 7 into two components: E'_G, or the reflected plane wave from a ground plane without an aperture, and E'_{RS}, the negative of the reflection from a thick wall or strip (reflected geometrical optics strip). The values of these components on S are given by

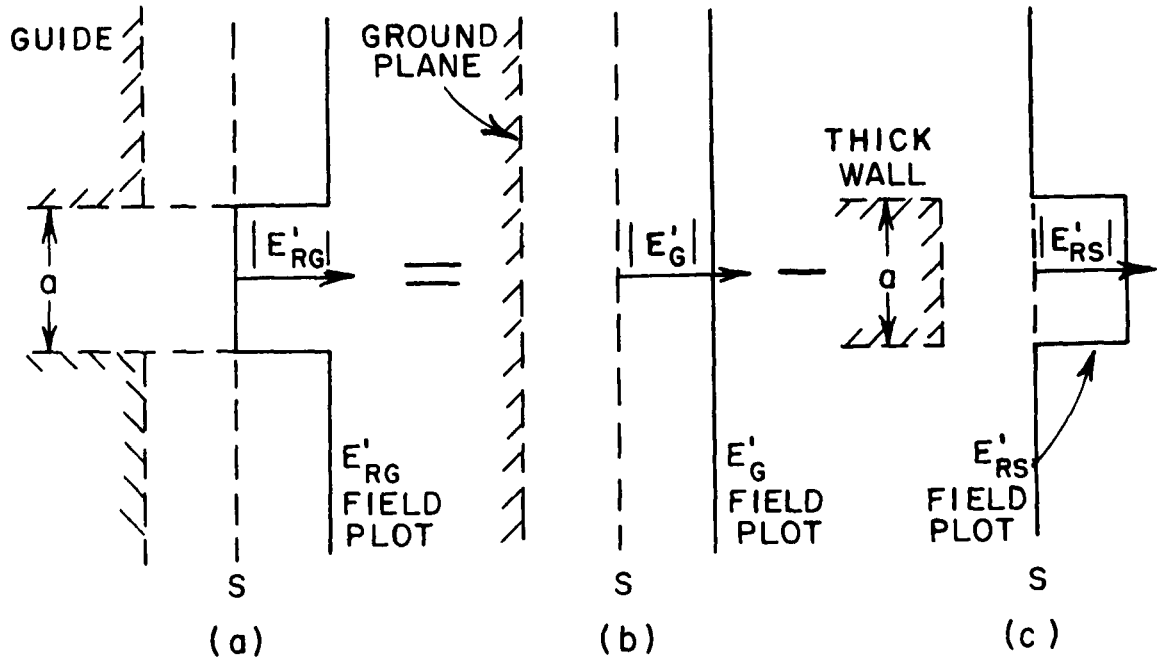

Fig. 7. Applications of superposition to the reflected geometrical optics components from the guide.

$$E'_G(y') = - e^{-jk(2f)} \quad \text{for all } y' , \tag{30}$$

and

$$E'_{RS}(y') = \begin{cases} e^{jk(2f)} & \text{for } 0 \geq y' \geq -a \\ 0 & \text{otherwise} \end{cases} . \tag{31}$$

with

$$E'_{RG}(y') = E'_G(y') + E'_{RS}(y') \quad . \tag{32}$$

Applying Eq. (21) to these components and integrating over S, it is seen that the plane wave component E_G, will still remain a plane wave at the observation plane located a distance d' away. The contributions of the reflected geometrical optics strip, E'_{RS}, is seen to be given by

$$E_{RS}(x, y) = 2 \int_{-a}^{0} E'_{RS}(0, y') \left. \frac{\partial G_o}{\partial x'} \right|_{x'=0} dy' \tag{33}$$

$$= \frac{e^{-jk(2f)}}{2j} \int_{-a}^{0} H_1^{(2)}(kr) \frac{kd}{r} \, dy' \quad .$$

Thus the total contribution from the reflected geometrical optics component at P(x, y) is given by

$$E_{RG}(x, y) = E_G(x, y) + E_{RS}(x, y) \quad , \tag{34}$$

where

$$E_G(x, y) = - e^{-jk[2f+x]} \quad . \tag{35}$$

D. Results

From Eqs. (20), (28), and (34), the total scattered field on the observation plane may be determined by

$$E_{TS} = E_D + E_{RD} + E_{RG} \tag{36}$$

$$= E_D + E_{RD} + E_G + E_{RS} \quad ,$$

where

E_{TS} = total scattered field,

E_D = direct diffraction contribution from the flaps,

E_{RD} = reflected diffraction contribution from the flaps,

E_{RG} = reflected geometrical optics component from the guide,

E_G = reflected plane wave from a ground plane without an aperture, and

E_{RS} = reflected geometrical optics strip or the negative of the reflection from a conducting wall.

A computer program in Fortran IV presented in Appendix I has been written to aid in the calculation of the scattered field. The results thus obtained are shown in Figs. 8 through 12 as a function of flap length for various values of f and d'. Figure 8 presents the magnitude of the scattered field on an observation plane located 3.0λ from the guide aperture for various flap lengths shorter than 0.6λ. It can be seen that $f = 0.3205\lambda$ yields the deepest dip in $|E_{TS}|$. Figure 9 gives the same data for f less than one wavelength while Fig. 10 supplies the cases for which $f > 1.0\lambda$. It can be seen from these results that optimum flap lengths, which give the deepest null, occur approximately once every $\lambda/2$, an observation in line with physical intuition. These optimum lengths for relatively short flaps are thus concluded to be $f = 0.3205\lambda$, 0.8205λ, and 1.3205λ.

Figure 11 presents $|E_{TS}|$ for $f = 0.3205\lambda$ observed at $d' = 2.0\lambda$, 5.0λ, and 10.0λ. From this result the dip obtained by the attachment of the flaps onto the guide aperture can thus be concluded to diminish as the observation distance d' is increased. At $d' = \infty$, of course, the

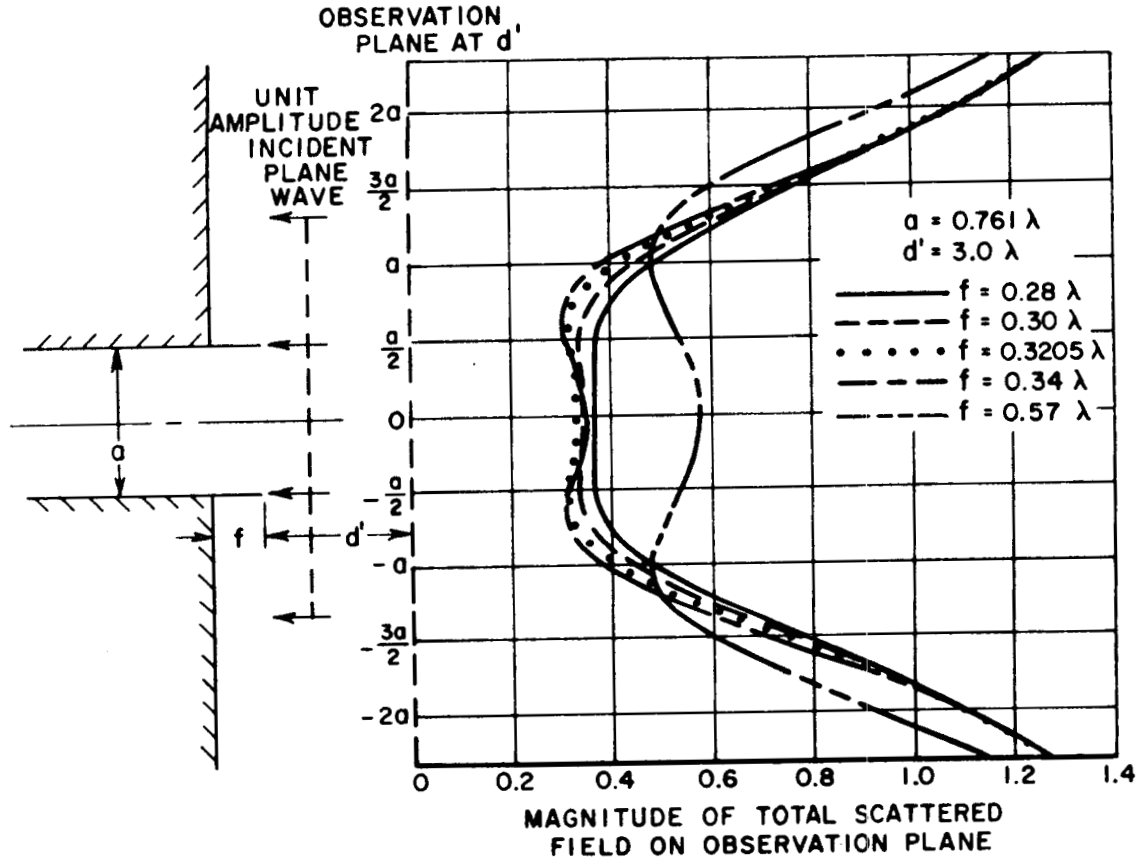

Fig. 8. $|E_{TS}|$ on an observation plane at d' = 3.0λ for flap lengths of 0.28λ, 0.30λ, 0.3205λ, 0.34λ and 0.57λ.

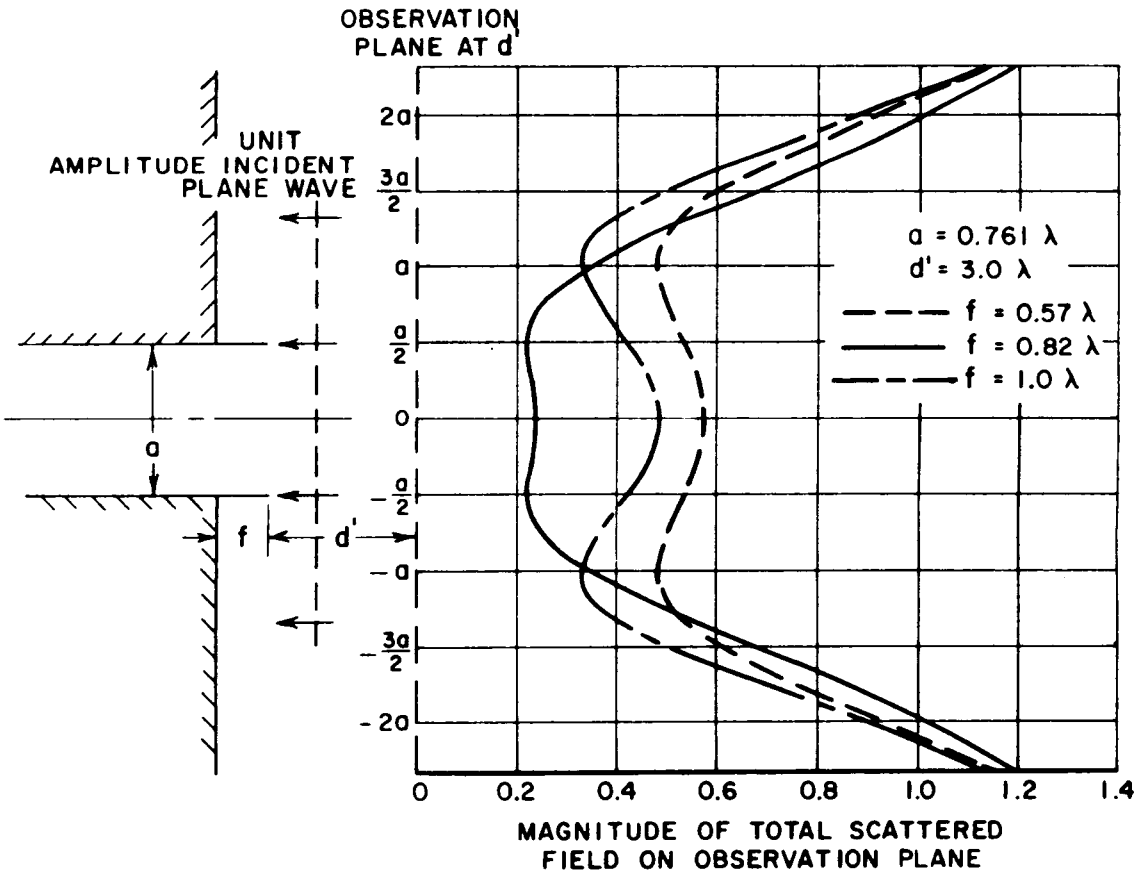

Fig. 9. $|E_{TS}|$ on an observation plane at d' = 3.0λ for flap lengths of 0.57λ, 0.82λ, and 1.0λ.

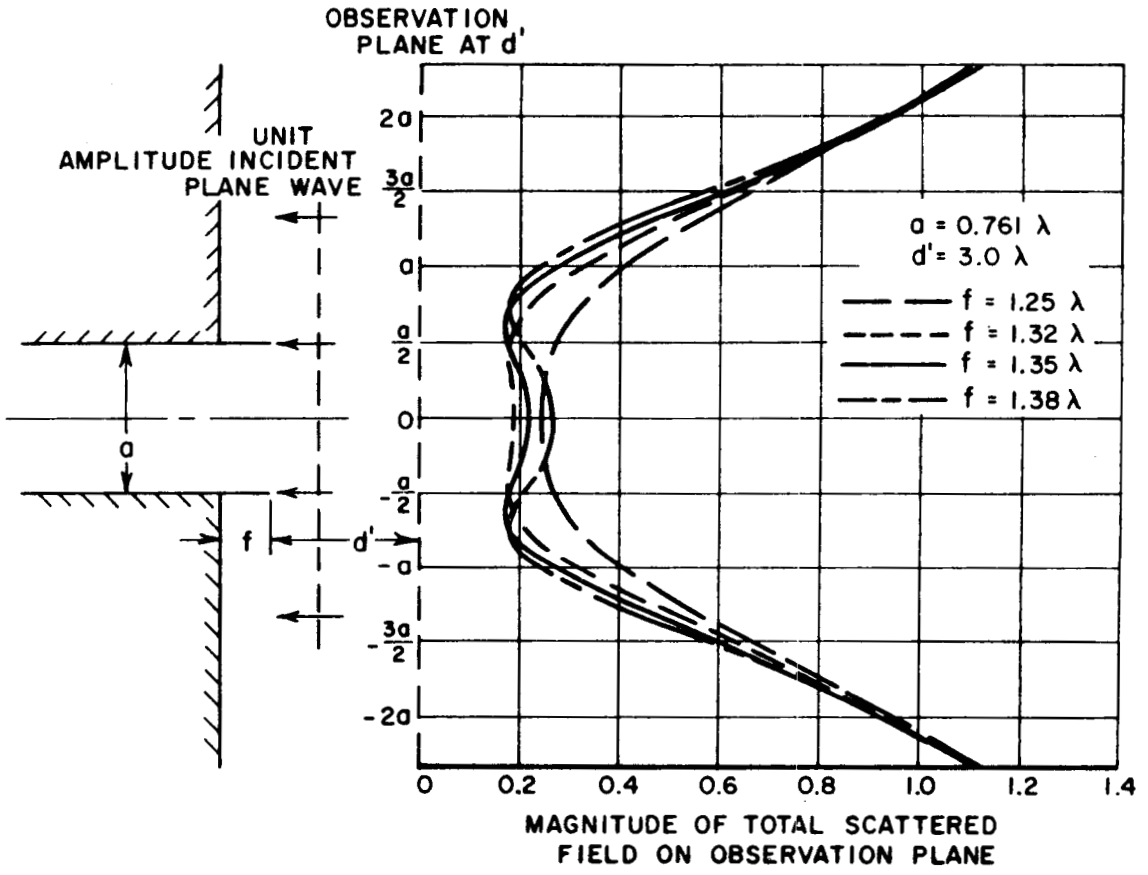

Fig. 10. $|E_{TS}|$ on an observation plane at d' = 3.0λ for flap lengths of 1.25λ, 1.32λ, 1.35λ, and 1.38λ.

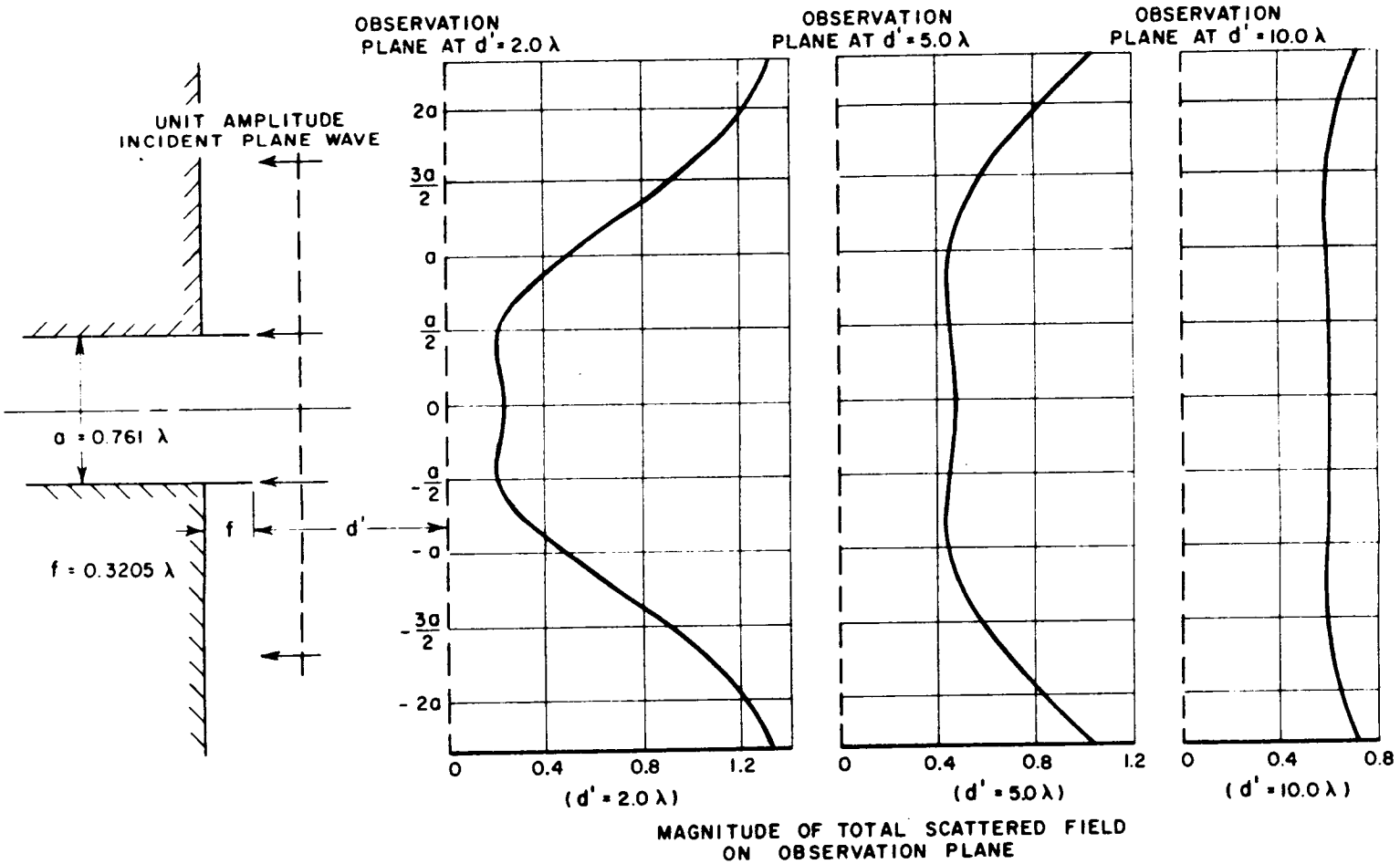

Fig. 11. $|E_{TS}|$ for the f = 0.3205λ case at observation plane distances of 2.0λ, 5.0λ, and 10.0λ.

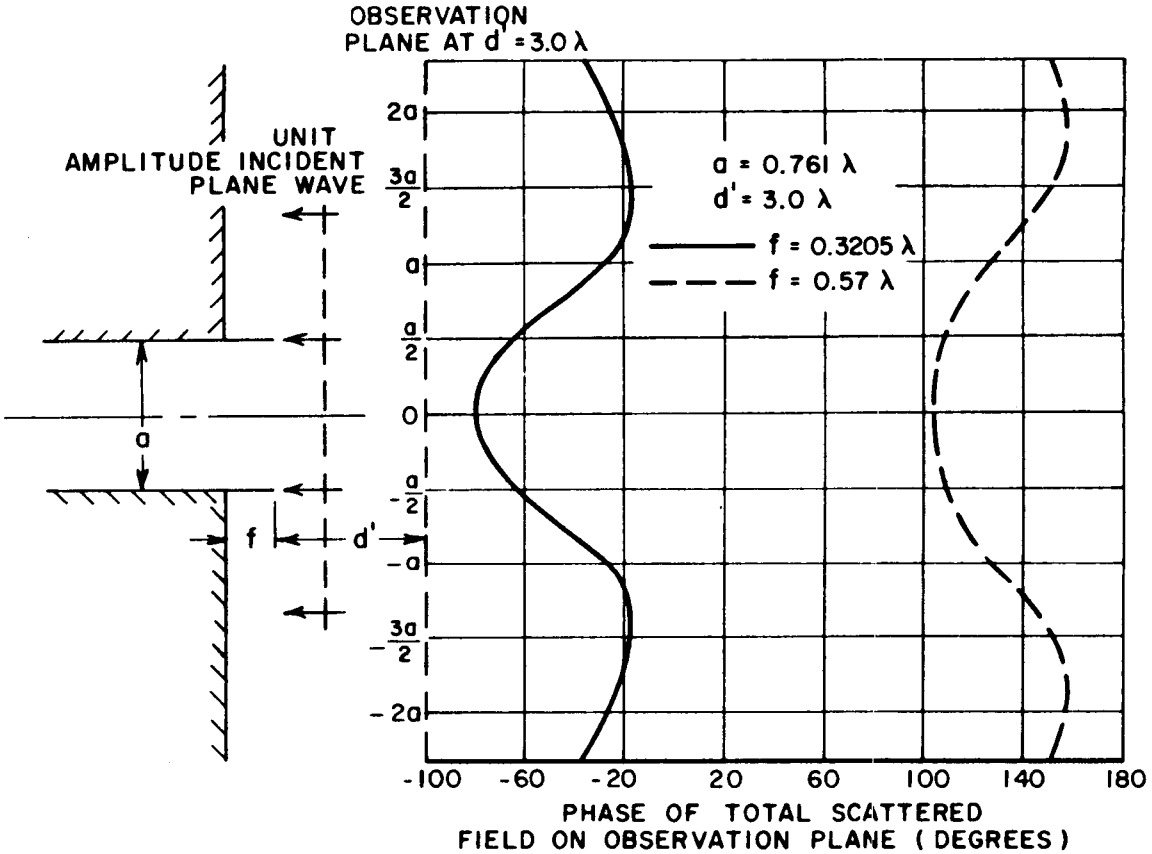

Fig. 12. Phase of E_{TS} on an observation plane at $d' = 3.0\lambda$ for flap lengths of 0.3205λ and 0.57λ.

presence of the aperture should have no effect on the scattered field which then becomes the reflected plane wave from a ground plane.

The phase of the scattered field is exemplified by the cases for which $f = 0.3205\lambda$, and 0.57λ, and $d' = 3.0$ as presented in Fig. 12

E. Equivalent Line Source Representations

The scattered field from the guide due to an incident plane wave may be seen both theoretically and numerically to be resolvable into cylindrical component waves. The components obtained in the previous sections can be treated as follows:

(1) E_G, the reflected plane wave from a ground plane without an aperture, can be identified as the geometrical optics reflection of the incident field by the ground plane

(2) E_D, the direct diffraction contribution from the flaps, actually seems to eminate from edges 1 and 2 and hence can be represented by an equivalent line source, V_D, located at the guide aperture center.

(3) $E_{RD} + E_{RS}$, the sum of the reflected diffraction contribution from the flaps and the reflected geometrical optics strip component, as seen by image theory, can be represented by an equivalent line source, V_R located at a distance $2f$ behind the guide aperture. The modal voltages of these equivalent sources are then obtained from Eq. (4) as

$$V_D = e^{jkd'} \sqrt{2\pi d'}\, E_D(d', -a/2), \tag{37}$$

and

$$V_R = e^{jk(d'+2f)} \sqrt{2\pi (d'+2f)}\, [E_{RD}(d', -a/2) + E_{RS}(d', -a/2)] \quad . \tag{38}$$

Numerical verification of these equivalent line source representations for the scattered field is given in Tables I and II for the cases in which $a = 0.761\lambda$, $f = 0.3205\lambda$, and $d' = 3.0\lambda$ and 10.0λ.

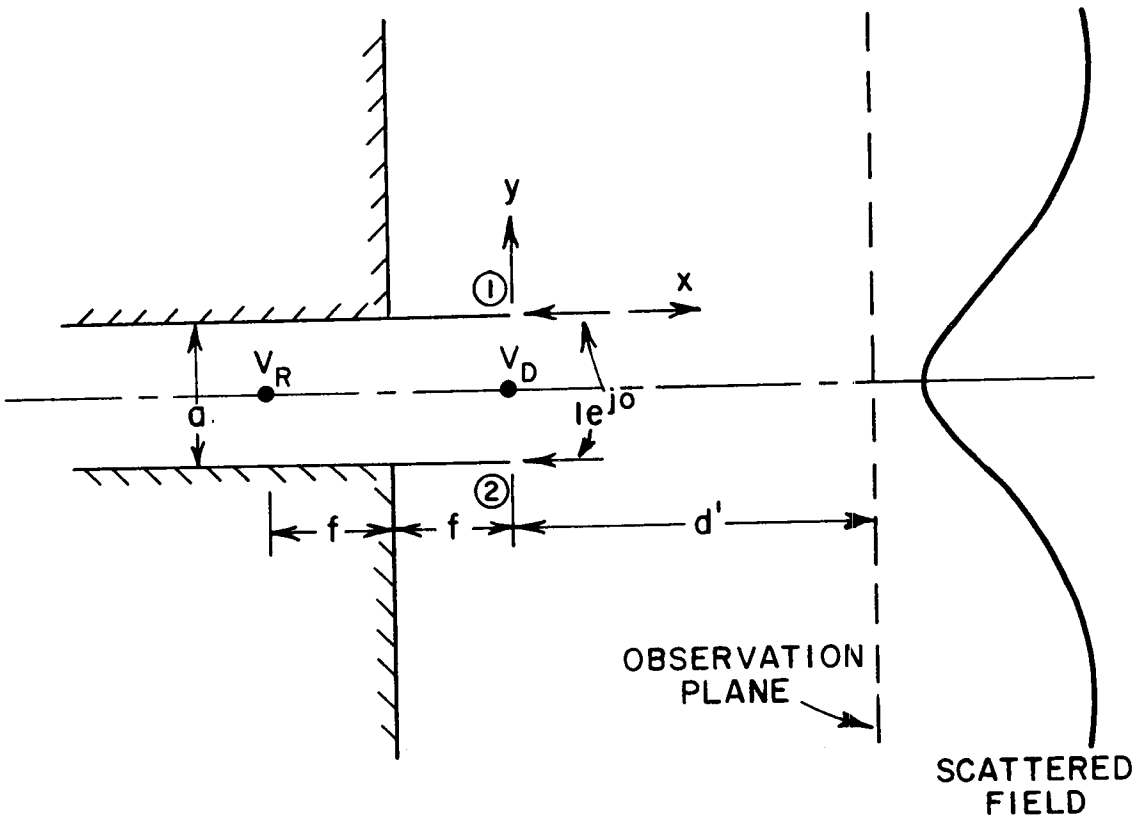

Fig. 13. Equivalent line source representations of the scattered field.

TABLE Ia

ACTUAL AND EQUIVALENT DIRECT DIFFRACTION CONTRIBUTIONS

($a = 0.761\lambda$, $f = 0.3205\lambda$, $d' = 3.0\lambda$)

	Actual Direct Diffraction Contribution E_D (Eq. 20)		Field from Equivalant Line Source V_D (Eq. 37)		
y	Magnitude	Phase (degrees)	Magnitude	Phase (degrees)	
-0.3805	0.14685	108.2	0.14685	108.2	Guide Center
-0.2537	0.14607	107.3	0.14679	107.2	
-0.1268	0.14376	104.4	0.14659	104.4	
0.0000	0.13999	99.7	0.14627	99.6	Guide Edge
0.1268	0.13489	93.2	0.14582	92.9	
0.2537	0.12859	84.8	0.14525	84.3	
0.3805	0.12128	74.7	0.14458	74.0	
0.5073	0.11316	62.8	0.14380	61.9	
0.6342	0.10441	49.3	0.14293	48.1	
0.7610	0.09524	34.1	0.14200	32.7	

TABLE Ib

ACTUAL AND EQUIVALENT REPRESENTATIONS FOR THE REFLECTED DIFFRACTION PLUS THE REFLECTED GEOMETRICAL OPTICS STRIP CONTRIBUTIONS
($a = 0.761\lambda$, $f = 0.3205\lambda$, $d' = 3.0\lambda$)

	Actual Reflected Diffraction plus Reflected Geometrical Optic Strip $E_{RD} + E_{RS}$ (Eqs. 28 and 33)		Field from Equivalent Line Source V_R (Eq. 38)		
y	Magnitude	Phase (degrees)	Magnitude	Phase (degrees)	
-0.3805	0.61048	150.1	0.61048	150.1	Guide Center
-0.2537	0.60856	149.3	0.61029	149.3	
-0.1268	0.60299	147.0	0.60974	146.9	
0.0000	0.59423	143.2	0.60882	142.9	Guide Edge
0.1268	0.58279	137.9	0.60755	137.4	
0.2537	0.56901	131.2	0.60593	130.3	
0.3805	0.55301	123.1	0.60399	121.8	
0.5073	0.53484	113.6	0.60173	111.7	
0.6342	0.51478	102.8	0.59917	100.1	
0.7610	0.49344	90.6	0.59634	87.2	

TABLE IIa

ACTUAL AND EQUIVALENT DIRECT DIFFRACTION CONTRIBUTIONS

($a = 0.761\lambda$, $f = 0.3205\lambda$, $d' = 10.0\lambda$)

	Actual Direct Diffraction Contribution E_D (Eq. 20)		Field from Equivalent Line Source V_D (Eq. 37)		
y	Magnitude	Phase (degrees)	Magnitude	Phase (degrees)	
-0.3805	0.08036	113.7	0.08036	113.7	Guide Center
-0.2537	0.08032	113.4	0.08035	113.4	
-0.1268	0.08020	112.5	0.08034	112.5	
0.0000	0.08001	111.1	0.08033	111.1	Guide Edge
0.1268	0.07974	109.1	0.08031	109.1	
0.2537	0.07940	106.5	0.08028	106.5	
0.3805	0.07898	103.3	0.08024	103.3	
0.5073	0.07849	99.5	0.08020	99.5	
0.6342	0.07793	95.2	0.08015	95.2	
0.7610	0.07729	90.3	0.08010	90.3	

TABLE IIb

ACTUAL AND EQUIVALENT REPRESENTATIONS FOR THE REFLECTED DIFFRACTION PLUS THE REFLECTED GEOMETRICAL OPTICS STRIP CONTRIBUTIONS

($a = 0.761\lambda$, $f = 0.3205\lambda$, $d' = 10.0\lambda$)

	Actual Reflected Diffraction plus Reflected Geometrical Optics Strip $E_{RD} + E_{RS}$ (Eq. 28 and 33)		Field from Equivalent Line Source V_R (Eq. 38)		
y	Magnitude	Phase (degrees)	Magnitude	Phase (degrees)	
-0.3805	0.35956	152.8	0.35956	152.8	Guide Center
-0.2537	0.35955	152.6	0.35955	152.5	
-0.1268	0.35948	152.0	0.35951	151.7	
0.0000	0.35920	150.8	0.35945	150.4	Guide Edge
0.1268	0.35860	149.1	0.35936	148.5	
0.2537	0.35757	146.8	0.35924	146.0	
0.3805	0.35615	143.8	0.35910	143.0	
0.5073	0.35447	140.2	0.35894	139.5	
0.6342	0.35269	135.9	0.35875	135.4	
0.7610	0.35093	131.1	0.35853	130.8	

It may be noted that the equivalent line source modal voltages, V_R and V_D, depend only on the amplitude of the incident field (unity amplitude plane wave assumed incident for Eqs. (37) and (38)) and is independent of the observation distance d'. This property will be useful in the reflection coefficient analysis discussed in the next section, where the same property is assumed for cylindrical wave incidence. The scattered field components associated with the presence of the aperture, i.e., those representable by the equivalent line sources V_R and V_D, may be thus expressed in general as

$$E_D = E^i K_D \frac{e^{-jkr_o}}{\sqrt{r_o}} \quad , \tag{39}$$

and

$$E_R = E_{RD} + E_{RS} = E^i K_R \frac{e^{-jkr_o}}{\sqrt{r_o}} \quad , \tag{40}$$

where E^i may be an incident plane wave of arbitrary amplitude and r_o is the observation distance. E_D is the equivalent direct diffraction contribution and E_R is the equivalent reflected contribution from the aperture. K_R and K_D may be regarded as constant scattering coefficients of a particular guide structure with their values obtainable through Eqs. (39) and (40) by making the substitutions $E^i = 1\, e^{j0}$, $r_o = d'$, and the values of E_D and E_R as exemplied in Tables I or II. The cases to be considered in the next section are: (1) $f = 0.3205\lambda$, $a = 0.761\lambda$; $K_D = 0.254 \angle 108.2°$; $K_R = 1.165 \angle 20.4°$; and (2) $f = 0.57\lambda$, $a = 0.761\lambda$; $K_D = 0.254 \angle 108.2°$; $K_R = 1.337 \angle 17.7°$.

III. REFLECTION COEFFICIENT ANALYSIS

In this section the reflection coefficient of the ground-plane-mounted TE_{01} mode parallel plate waveguide with conducting flaps attached to the aperture and illuminating a conducting sheet as shown in Fig. 1 is analyzed in a manner similar to that employed in Ref. 2. By the wedge diffraction method the reflection coefficient of the waveguide is the superposition of the free space reflection coefficient, Γ_s, and the reflection coefficient caused by the presence of the conducting sheet, Γ_p. The free space reflection coefficient for this guide structure may be approximated by the solution for the thin walled case given in Ref. 5. However, Γ_s in general is quite small and in practice can be matched out;[8] therefore,

it will not be included in the subsequent discussions. The reflection due to the sheet is analyzed in terms of successive contributions or bounces which describe the interaction of the fields between the guide and the sheet.

Formulating the reflection from the sheet in terms of successive bounces, the first bounce wave is the free space radiation from the waveguide, Eq. (9), which reflects from the sheet back onto the waveguide. The first bounce wave then scatters from the guide producing a second bounce wave which propagates toward the reflecting sheet. The second bounce wave in turn reflects from the sheet back onto the waveguide giving rise to a third bounce wave, and so on to higher order bounces. Each bounce produces a contribution to the reflected TE_{01} mode in the waveguide.

A. First Bounce

As stated by Eq. (10), calculations show that in the region of the projected guide cross section the free space wave radiated from the guide may be represented by an isotropic cylindrical wave from a line source located at the center of the guide aperture. This and subsequent

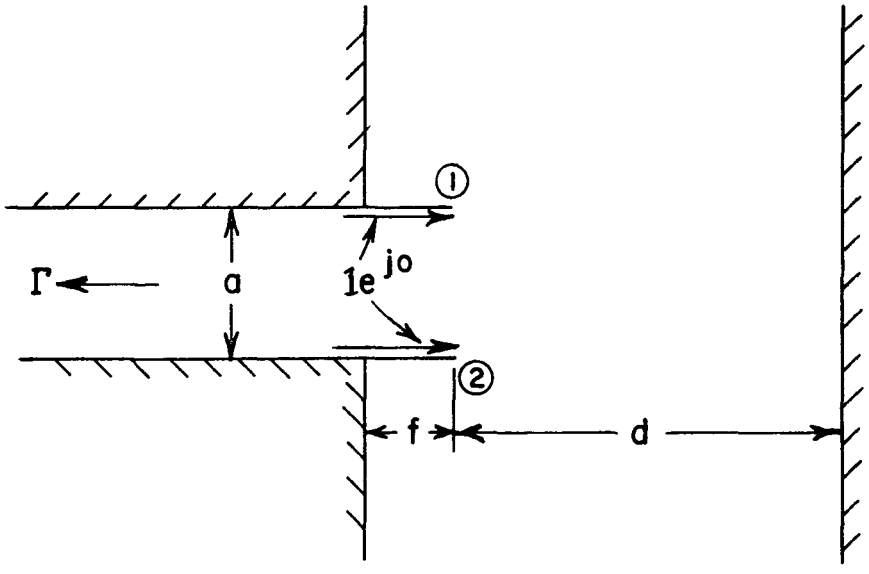

Fig. 14. The reflection coefficient of a TE_{01} mode ground plane mounted guide with aperture flaps illuminating a conducting sheet.

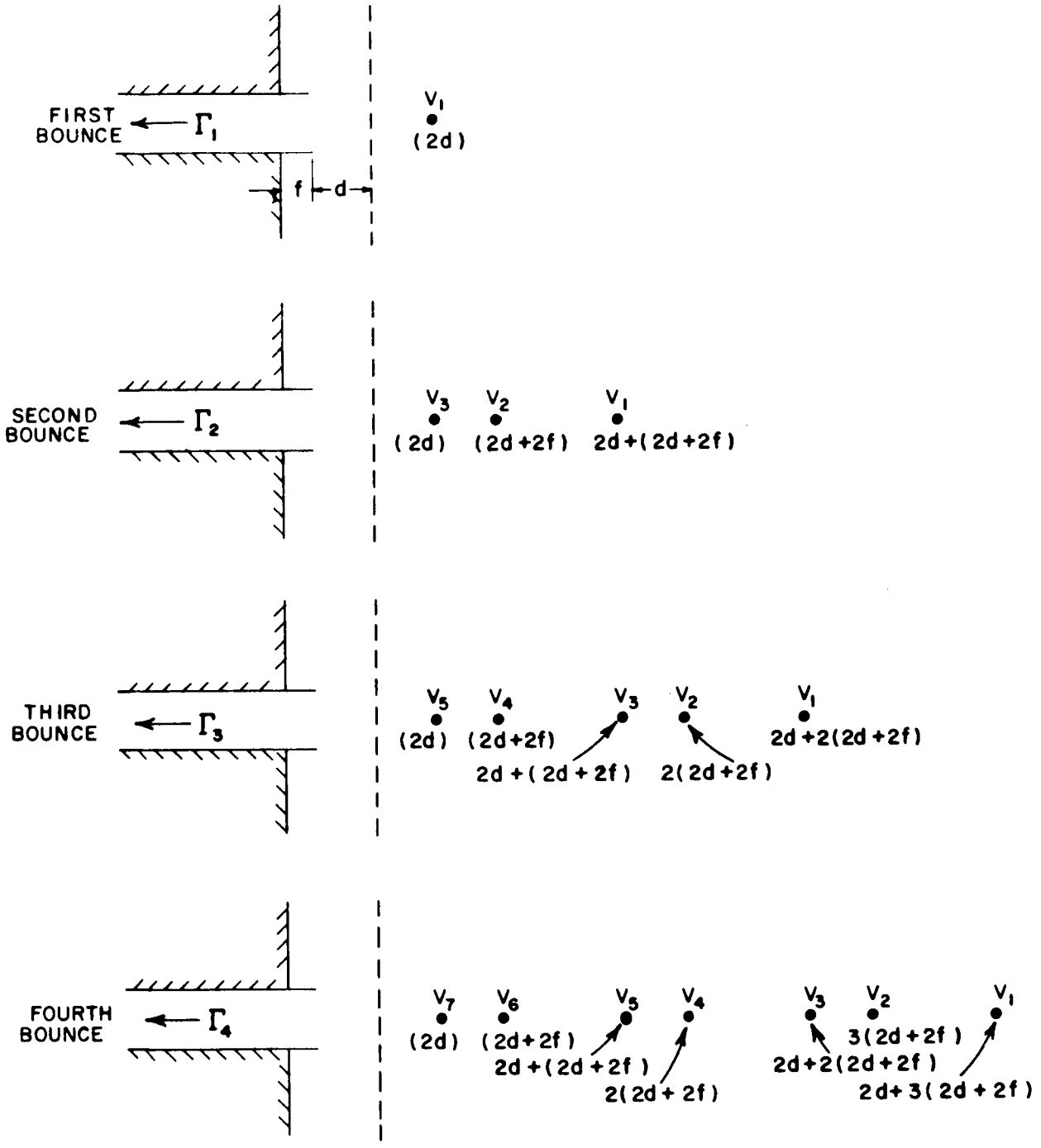

Fig. 15. Equivalent line source locations for the multiple bounce diagram.

approximations in this report are valid provided the observation distances are sufficiently removed from the aperture. In general, a rule of thumb would be to keep the conducting sheet distance d always greater than a, the guide width, for $a < \lambda$.

By image theory the equivalent line source representing the first bounce wave may thus be seen from Fig. 15a to be located at a distance 2d from the guide aperture and with modal voltage V_1 given by

$$V_1 = - R_T(\theta = 0) \frac{e^{-j\pi/2}}{\sqrt{k}} \quad , \tag{41}$$

where $R_T(\theta = 0)$ is the on axis ray from Eq. (9). The minus sign arises from the reflection by the conducting sheet. The field incident on the guide from the first bounce equivalent line source is then given by

$$E_1^i = V_1 \frac{e^{-jk(2d)+j\pi/4}}{\sqrt{2\pi(2d)}} = - R_T(\theta=0) \frac{e^{-j\pi/2}}{\sqrt{k}} \frac{e^{-jk(2d)+j\pi/4}}{\sqrt{2\pi(2d)}} \quad . \tag{42}$$

Using the line source to waveguide coupling expression given in Eq. (12), the first bounce reflection coefficient is given by

$$\Gamma_1 = \frac{V}{V_o} = \frac{\sqrt{\lambda}}{2a\cos A_o} \frac{1}{2\pi\sqrt{k}} e^{-j\pi/4} R_T(\theta=0) V_1 \frac{e^{-jk(2d)}}{\sqrt{2d}} \tag{43}$$

$$= C V_1 \frac{e^{-jk(2d)}}{\sqrt{2d}} \quad .$$

B. Second Bounce

The first bounce equivalent line source field scatters from the guide producing a second bounce wave. It was seen in Section II that the scattered field from the guide for plane wave incidence may be resolved into the geometrical optics component and two cylindrical component waves associated with the presence of the aperture. The aperture components of the scattered field resulting from an incident cylindrical wave, however, depends only on the value of the incident field and is independent of the source location provided the source is sufficiently

removed from the guide. For the case of cylindrical wave incidence, the aperture component of the scattered wave is, therefore, the same as that for plane wave incidence with the plane wave field equal to the incident field of the cylindrical wave at the waveguide aperture.

The geometrical optics component of the second bounce wave reflects from the sheet back onto the waveguide such that it may be represented by the line source V_1 located at a distance $[2d + (2d+2f)]$ from the guide aperture, as shown in Fig. 15b. The aperture components of the second bounce wave reflect onto the waveguide as described by the line sources V_2 and V_3 in Fig. 15b The values of V_2 and V_3 are obtained by equating the radiated fields with those of the aperture components in Eqs. (39) and (40). Thus

$$(44a) \qquad E_R = V_2 \frac{e^{-jkr_o + j\pi/4}}{\sqrt{2\pi r_o}} = - E^i K_R \frac{e^{-jkr_o}}{\sqrt{r_o}} \quad ,$$

and

$$(44b) \qquad E_D = V_3 \frac{e^{-jkr_o + j\pi/4}}{\sqrt{2\pi r_o}} = - E^i K_D \frac{e^{-jkr_o}}{\sqrt{r_o}} \quad ,$$

where the minus sign again results from the reflection off the conducting sheet and E^i is the incident field of the illuminating line source V_1 at the guide aperture given by Eq. (42). Hence the value of V_2 and V_3 are given, respectively, by

$$(45a) \qquad V_2 = - V_1 K_R \frac{e^{-jk(2d)}}{\sqrt{2d}} \quad ,$$

and

$$(45b) \qquad V_3 = - V_1 K_D \frac{e^{-jk(2d)}}{\sqrt{2d}} \quad .$$

The corresponding second bounce reflection coefficient is then given by the modal voltage induced by V_1, V_2, and V_3 as shown in Fig. 15b

$$(46) \qquad \Gamma_2 = C\left[V_1 \frac{e^{-jk[2d+(2d+2f)]}}{\sqrt{2d+(2d+2f)}} + V_2 \frac{e^{-jk(2d+2f)}}{\sqrt{2d+2f}} + V_3 \frac{e^{-jk(2d)}}{\sqrt{2d}}\right]$$

C. Multiple Bounces

The generation of the third bounce is similar to the generation of the second bounce with the line source locations as shown in Fig. 15c and modal voltages given by

$$(47) \qquad V_4 = -K_R\left[V_1 \frac{e^{-jk[2d+(2d+2f)]}}{\sqrt{2d+(2d+2f)}} + V_2 \frac{e^{-jk(2d+2f)}}{\sqrt{2d+2f}} + V_3 \frac{e^{-jk(2d)}}{\sqrt{2d}}\right]$$

$$(48) \qquad V_5 = -K_D\left[V_1 \frac{e^{-jk[2d+(2d+2f)]}}{\sqrt{2d+(2d+2f)}} + V_2 \frac{e^{-jk(2d+2f)}}{\sqrt{2d+2f}} + V_3 \frac{e^{-jk(2d)}}{\sqrt{2d}}\right].$$

The third bounce reflection coefficient contribution is given by

$$(49) \qquad \Gamma_3 = C\left[V_1 \frac{e^{-jk[2d+2(2d+2f)]}}{\sqrt{2d+2(2d+2f)}} + V_2 \frac{e^{-jk[2(2d+2f)]}}{\sqrt{2(2d+2f)}}\right.$$

$$+ V_3 \frac{e^{-jk[2d+(2d+2f)]}}{\sqrt{2d+(2d+2f)}} + V_4 \frac{e^{-jk[2d+2f]}}{\sqrt{2d+2f}}$$

$$\left. + V_5 \frac{e^{-jk(2d)}}{\sqrt{2d}}\right]$$

Generalizing, the n-th bounce wave is given by (2n-1) cylindrical wave components with sources V_1 at $[2d+(n-1)(2d+2f)]$, V_2 at $[(n-1)(2d+2f)]$, V_3 at $[2d+(n-2)(2d+2f)]$, V_4 at $[(n-2)(2d+2f)]$, -----$V_{(2n-2)}$ at $[2d+2f]$, and $V_{(2n-1)}$ at $[2d]$. The sources associated with this bounce are given by

$$(50) \qquad V_{(2n-2)} = -K_R \left[\sum_{m=1}^{n-1} V_{(2m-1)} \frac{e^{-jk[2d+(n-m-1)(2d+2f)]}}{\sqrt{2d+(n-m-1)(2d+2f)}} + \sum_{m=1}^{n-2} V_{(2m)} \frac{e^{-jk[(n-m-1)(2d+2f)]}}{\sqrt{(n-m-1)(2d+2f)}} \right]$$

and

$$(51) \qquad V_{(2n-1)} = -K_D \left[\sum_{m=1}^{n-1} V_{(2m-1)} \frac{e^{-jk[2d+(n-m-1)(2d+2f)]}}{\sqrt{2d+(n-m-1)(2d+2f)}} + \sum_{m=1}^{n-2} V_{(2m)} \frac{e^{-jk[(n-m-1)(2d+2f)]}}{\sqrt{(n-m-1)(2d+2f)}} \right] .$$

The n-th bounce contribution to the reflection coefficient is thus given by

$$(52) \qquad \Gamma_n = C \left[\sum_{m=1}^{n} V_{(2m-1)} \frac{e^{-jk[2d+(n-m)(2d+2f)]}}{\sqrt{2d+(n-m)(2d+2f)}} + \sum_{m=1}^{n-1} V_{(2m)} \frac{e^{-jk[(n-m)(2d+2f)]}}{\sqrt{(n-m)(2d+2f)}} \right] .$$

The total reflection coefficient due to the reflecting sheet or plate is given by

$$(53) \qquad \Gamma_p = \sum_{n=1}^{\infty} \Gamma_n \quad .$$

D. Results

The total reflection coefficient, Γ_p due to the conducting sheet, as given in Eq. (53), was calculated as a function of the reflector spacing d for two different flap lengths with the aid of the Fortran IV computer program presented in Appendix II. The flap lengths chosen were 0.3205λ, an optimum length determined from the scattering program to give the deepest null, and 0.57λ, a non-optimal value. For both cases, a guide width of 0.761λ was used. The results thus obtained are as presented in Figs. 16 through 18 with the inclusions of up to 300 bounces.

Figure 16 compares the magnitude of Γ_p for the two flap lengths along with the reflection coefficient from the first bounce wave Γ_1. For both cases, the behavior of $|\Gamma_p|$ is quite like that observed in Ref. 2 for a TEM mode ground plane mounted guide (without flaps). $|\Gamma_p|$ is seen to oscillate about Γ_1 with a period of $\lambda/2$ in d. At values of d for which f + d = multiples of $\lambda/2$, the reflection coefficient is seen to rise to a sharp peak. This is exactly analogous to the resonance behavior observed in Ref. 2 for cavity spacings equal to $n\lambda/2$, where unity magnitude reflection coefficients were observed. From the basic nature of the problem of a TE_{01} ground-plane-mounted guide without flaps illuminating a conducting sheet, it is expected that the reflection coefficient for this problem will have the same fundamental behavior near critical values of reflector spacing $d = n\lambda/2$ as that for the TEM mode. Thus it is expected that complete reflection will occur at $d = n\lambda/2$ for the TE_{01} mode problem without flaps. The presence of the flaps eliminates complete reflection as can be seen from the results in Fig. 16. In fact, the optimum flap length of 0.3205λ can be seen to yield smaller oscillations in $|\Gamma_p|$ than that from $f = 0.57\lambda$, with a significant reduction in the peak values. For both cases, the peaks remain constant as d increases, an observation in line with that observed in Ref. 2.

The phase of Γ_p for the two flap lengths is shown in Fig. 17 with the phase of Γ_1. Figures 18a and 18b give the magnitude and phase of Γ_p for the $f = 0.3205\lambda$ case with large values of d. The same maximum value is observed in the sharp peak of $|\Gamma_p|$ at $d = 10.1795\lambda$ as was observed at smaller values of d. It is believed that the peak values will not diminish irregardless of the size of d due to the idealized geometry assumed, namely, infinite ground planes and conducting sheets.

From the data thus obtained, it can be seen that the presence of the flaps causes a considerable reduction in the amplitude of the oscillations in $|\Gamma_p|$. From the unity reflection case observed for the guide without flaps, the new structure is seen to offer lower peaks, especially at optimum flap lengths. Even though the monotone curve of $|\Gamma_p|$ vs d,

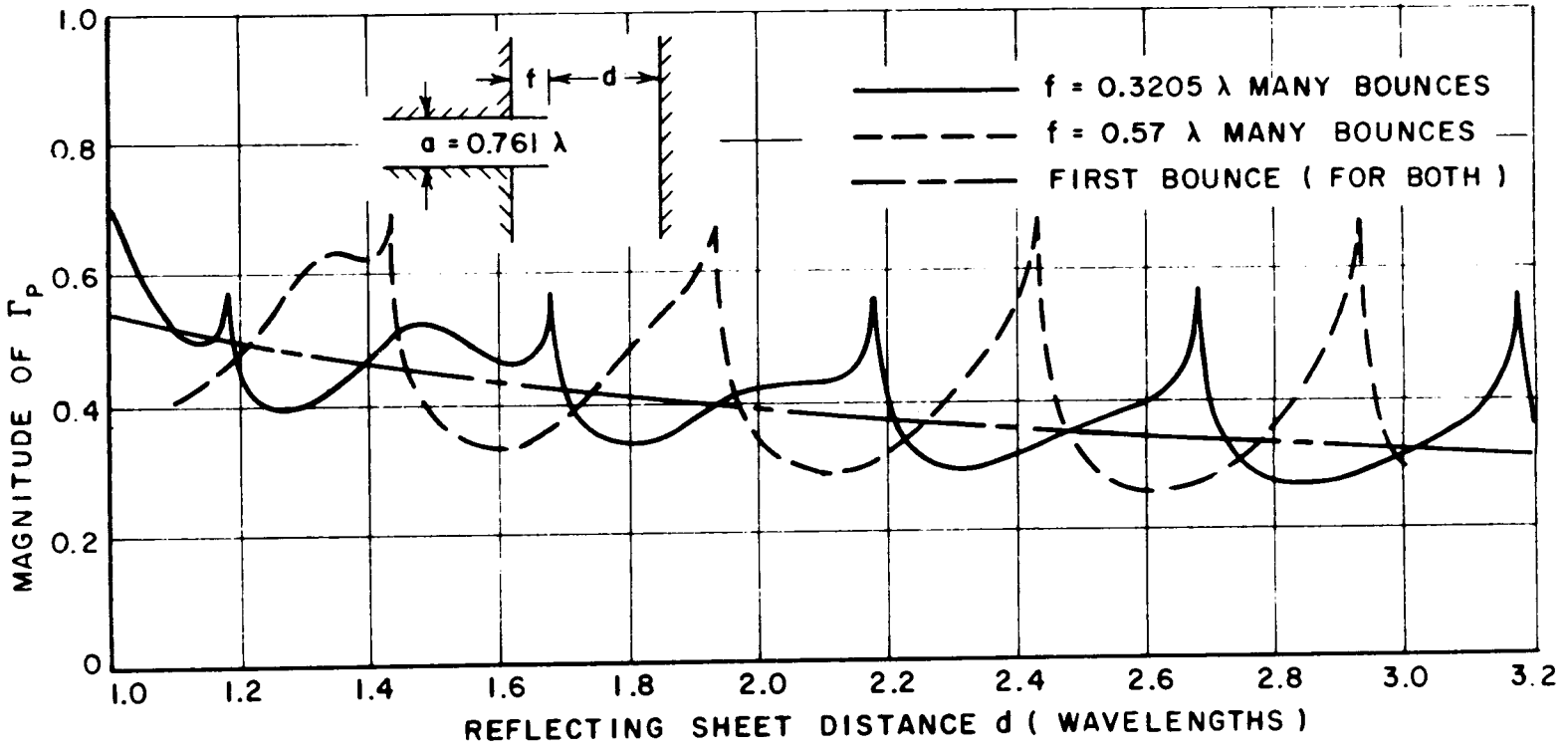

Fig. 16. The reflection coefficient magnitude for guides with flaps.

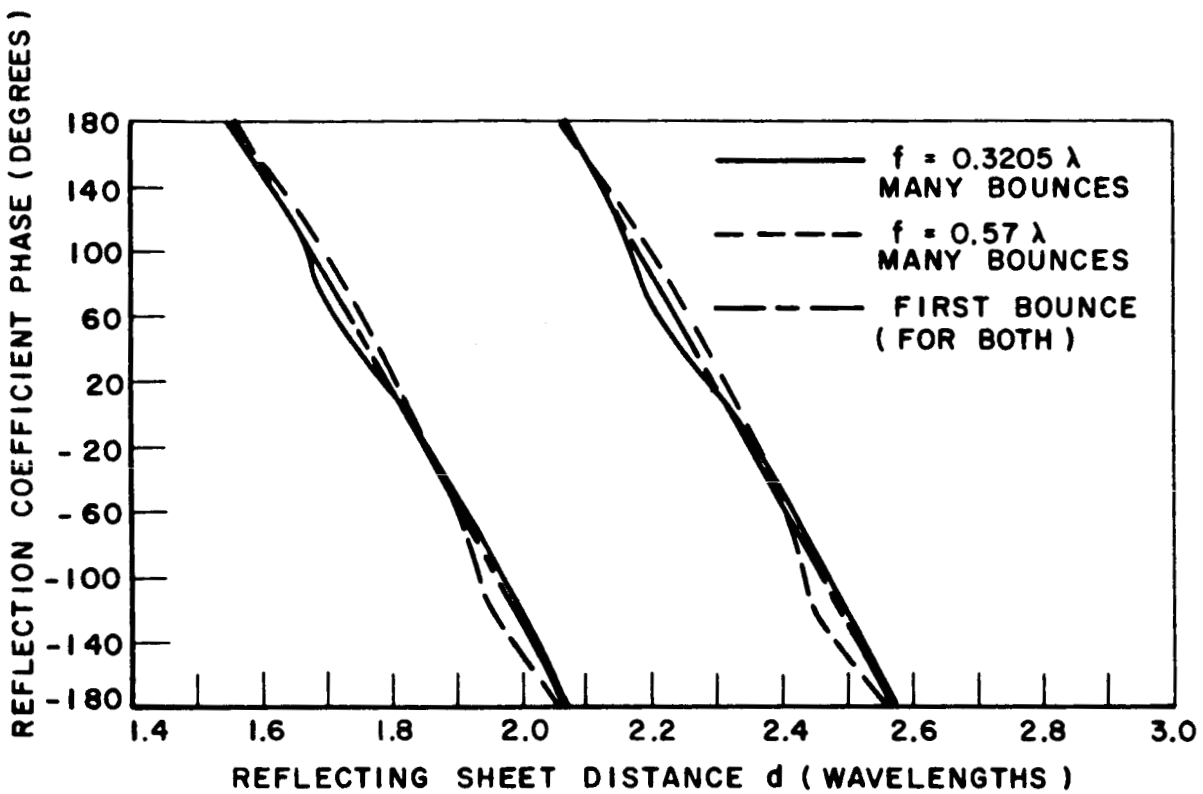

Fig. 17. Phase of Γ_p.

suitable for reflectometer antennas, was not obtained, this analysis nevertheless quantitatively predicts the best result that can be obtained with simple flaps.

IV. CONCLUSIONS

The influence of conducting flaps on the reflection coefficient of a ground-plane mounted TE_{01} mode parallel-plate waveguide illuminating a conducting sheet has been analyzed. The backscatter from the guide structure was obtained by applications of wedge diffraction and surface integration techniques. The reflection coefficient was then obtained through

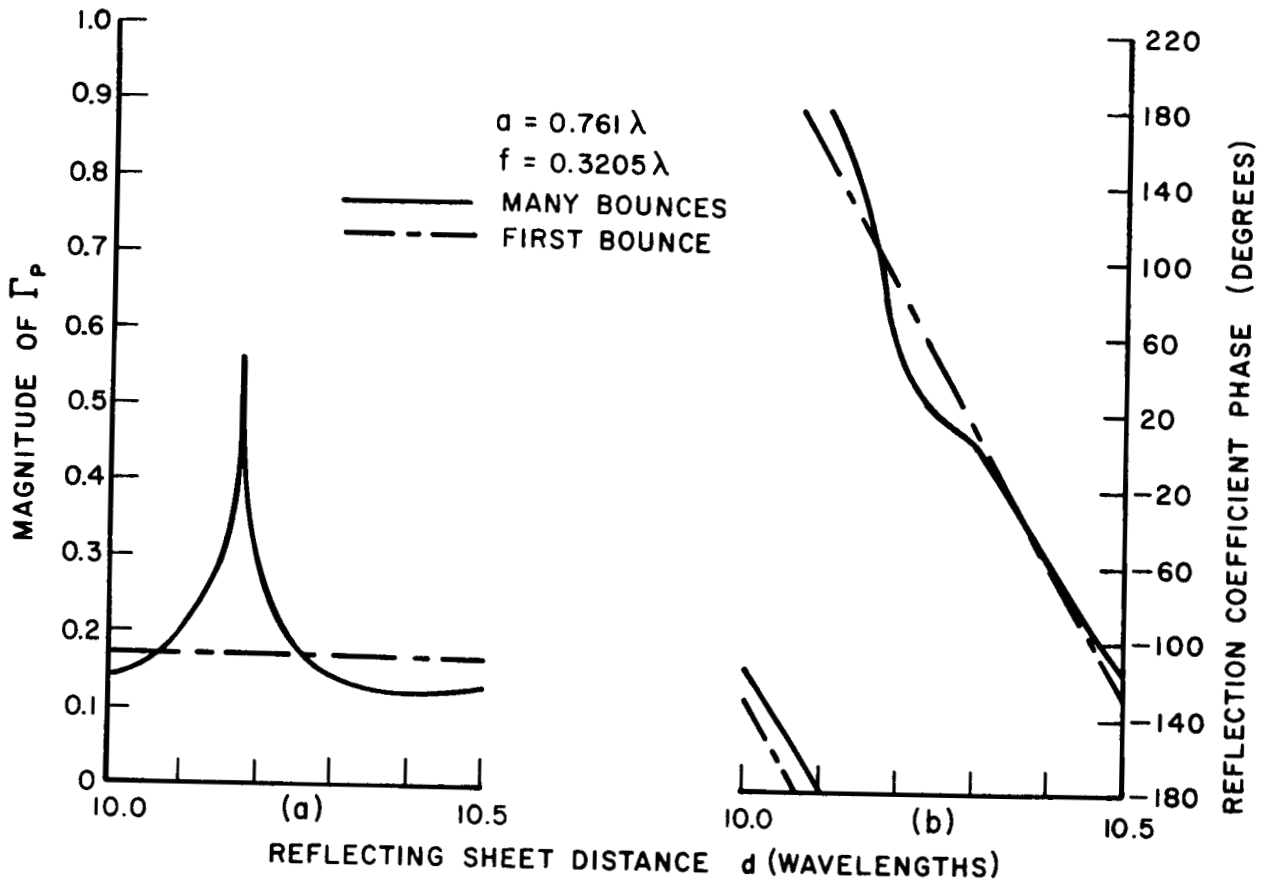

Fig. 18. (a) $|\Gamma_p|$ for larger d
(b) Phase of Γ_p for larger d.

an iterative multiple bounce procedure that describes the interactions between the guide and the reflector.

This analysis was motivated by the need to improve the design of reflectometer antennas which are used in plasma diagnostic measurements. Previous analyses and measurements have shown that a reflecting surface in front of the antenna will usually produce large interactions between the surface and the antenna; this results in large oscillations in the reflection coefficient as a function of the spacing between the two structures.

The results of this analysis show that the presence of flaps at edges of the antenna aperture can significantly reduce the oscillations in the

reflection coefficient. Optimum flap lengths can also be determined as those lengths which produce the greatest reduction in the on-axis backscatter from the ground-plane-mounted guide.

Though only thin planar flaps are used in this analysis, extensions may be easily made to other flap geometries which may yield lower backscatter and hence a more monotone response.

One possible application of the results from this analysis would be in reducing radar echo areas of slot arrays.

ACKNOWLEDGEMENTS

The authors wish to thank Prof. J.H. Richmond for providing the Hankel function subroutine and Mr. E.L. Pelton for supplying the integration subroutine.

REFERENCES

1. Tsai, L.L., "The Reflection Coefficient of a TEM Mode Parallel-Plate Waveguide Illuminating a Perfectly Reflecting Sheet," Report 2143-1, 25 August 1966, Antenna Laboratory, The Ohio State University Research Foundation; prepared under Grant NGR-36-008-048, National Aeronautics and Space Administration, Office of Grants and Research Contracts, Washington, D.C.

2. Tsai, L.L., and Rudduck, R.C., "The Reflection Coefficient of a Ground-Plane Mounted TEM Mode Parallel-Plate Waveguide Illuminating a Conducting Sheet," (ElectroScience Laboratory report in process).

3. Semiannual Status Report, Report 2143-3, 9 June 1967, Electro-Science Laboratory, The Ohio State University Research Foundation; prepared under Grant NGR-36-008-048, National Aeronautics and Space Administration, Washington, D.C.

4. Dybdal, R.B., Rudduck, R.C., and Tsai, L.L., "Mutual Coupling Between TEM and TE_{01} Parallel-Plate Waveguide Aperture," IEEE Transactions on Antennas and Propagation, Vol. AP-14, No. 5, (September 1966), pp. 574-580.

5. Rudduck, R.C., and Tsai, L.L., "Aperture Reflection Coefficient of TEM and TE_{01} Mode Parallel-Plate Waveguides," IEEE Transactions on Antennas and Propagation, Vol. AP-16, No. 1, (January 1968) pp. 83-89.

6. Wu, D.C.F., Tsai, L.L., and Rudduck, R.C., "Broadside Radiation of Parallel-Plate Waveguides," (ElectroScience Laboratory report in process).

7. Rudduck, R.C., "Application of Wedge Diffraction to Antenna Theory," Report 1691-13, 30 June 1965, Antenna Laboratory, The Ohio State University Research Foundation; prepared under Grant NsG-448, National Aeronautics and Space Administration, Office of Grants and Research Contracts, Washington, D.C.

8. Burnside, W.D., "The Reflection Coefficient of a TEM Mode Symmetric Parallel-Plate Waveguide Illuminating a Lossless Dielectric Layer," Report 1691-25, March 1968, ElectroScience Laboratory, The Ohio State University Research Foundation; prepared under Grant NsG-448, National Aeronautics and Space Administration, Office of Grants and Research Contracts, Washington, D.C.

9. Wu, D.C.F., "The TEM Radiation Pattern of a Thin-Walled Parallel-Plate Waveguide Analyzed by a Surface Integration Technique," Report 1691-23, 20 September 1967, ElectroScience Laboratory, The Ohio State University Research Foundation; prepared under Grant NsG-448, National Aeronautics and Space Administration, Washington, D.C.

10. Pelton, E.L., Wu, D.C.F., and Rudduck, R.C., "The TEM Radiation Pattern of a Ground-Plane Mounted Parallel-Plate Waveguide Analyzed by a Surface Integration Technique," (ElectroScience Laboratory report in process).

11. Hansen, R.C., Microwave Scanning Antennas, Vol. I, Academic Press Inc. (1966), pp. 5-9.

APPENDIX I

The computation of the backscatter from the guide for plane wave incidence given in Section II was aided by the Fortran IV computer program given below. The parameters used in the program are as shown in Fig. 19. The scattered field contributions are: ETD, the direct diffraction component; EG, the reflected geometrical optics strip component; and ETP, the reflected diffraction component.

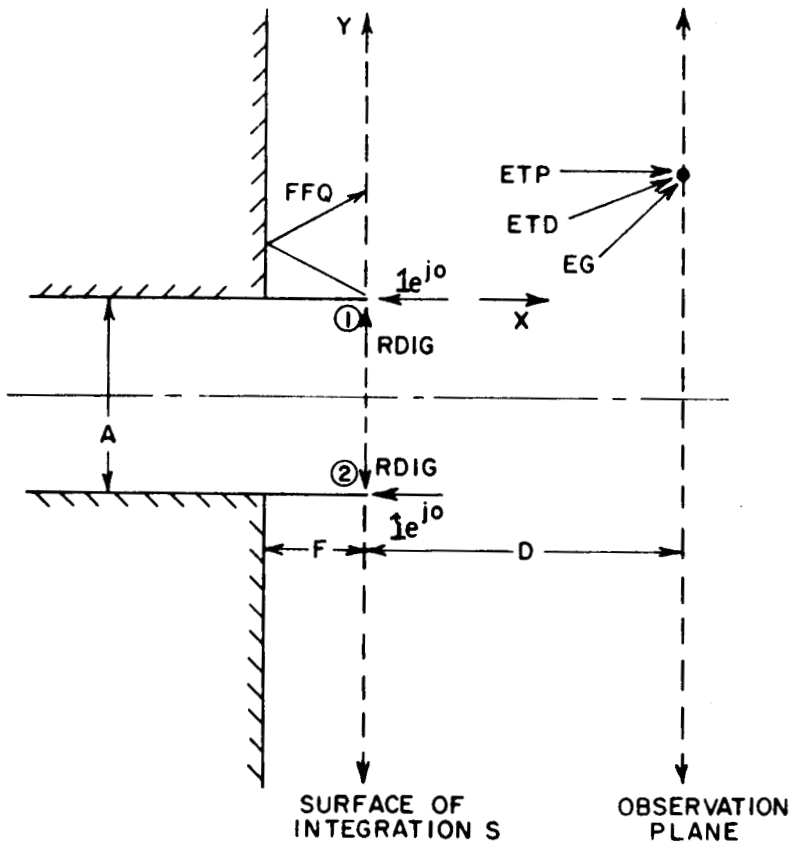

Fig. 19. Backscatter from the guide with plane wave incidence.

```
$EXECUTE        PUFFT
$PUFFT    500
C       TE01 FLAP GUIDE PROBLEM BY HYBRID METHOD WITH SURFACE INTEGRATION
        DIMENSION ETDR(100),ETDI(100),ETPR(100),ETPI(100),BTPR(100),BTPI(1
       200),EGR(100),EGI(100)
        COMPLEX PFT,ED1,ED2,CTEMP,EDD1,EDD2
        COMPLEX CTEMP1,CTEMP2
        TEMPA=1000.0
        TEMPD=1000.0
        PI=3.1415927
        TPI=2.0*PI
        PFT=CEXP(CMPLX(0.0,-PI/4.0))/TPI
  10    READ (5,11) A,F,D,NF
  11    FORMAT (3F10.4,I5)
        IF (NF.EQ.0) GO TO 500
        DA=A/6.0
        RD1G=-SQRT(2.0)
        WRITE (6,13) A,F,D
  13    FORMAT (//20X,3HA= ,F10.4,3HF= ,F10.4,3HD= ,F10.4//6X,1HY,12X,3HED
       21,17X,3HED2,16X,4HEDD1,16X,4HEDD2,17X,3HETD/)
        IF (TEMPD.EQ.D.AND.TEMPA.EQ.A) GO TO 200
        Y=-A/2.0
        DO 100 I=1,NF
        R1=SQRT(D*D+Y*Y)
        ALPH1=180.0/PI*ATAN2(Y,D)
        R2=SQRT(D*D+(Y+A)*(Y+A))
        ALPH2=180.0/PI*ATAN2(Y+A,D)
        CALL VB (RVB1,UVB1,R1,ALPH1,2.0)
        TEMP=360.0+ALPH1
        CALL VB (RVB2,UVB2,R1,TEMP,2.0)
        ED1=CMPLX(RVB1-RVB2,UVB1-UVB2)
        TEMP=-ALPH2
        CALL VB (RVB1,UVB1,R2,TEMP,2.0)
        TEMP=360.0-ALPH2
        CALL VB (RVB2,UVB2,R2,TEMP,2.0)
        ED2=CMPLX(RVB1-RVB2,UVB1-UVB2)
        TEMP1=A*R1/(A+R1)
        TEMP2=A*R2/(A+R2)
        CTEMP=CEXP(CMPLX(0.0,TPI*(TEMP1-R1-A)))/SQRT(R1+A)
        TEMP=90.0+ALPH1
        CALL VB (RVB1,UVB1,TEMP1,TEMP,2.0)
        TEMP=270.0+ALPH1
        CALL VB (RVB2,UVB2,TEMP1,TEMP,2.0)
        EDD1=RD1G*PFT*CTEMP*CMPLX(RVB1-RVB2,UVB1-UVB2)
        CTEMP=CEXP(CMPLX(0.0,TPI*(TEMP2-R2-A)))/SQRT(R2+A)
        TEMP=90.0-ALPH2
        CALL VB (RVB1,UVB1,TEMP2,TEMP,2.0)
        TEMP=270.0-ALPH2
        CALL VB (RVB2,UVB2,TEMP2,TEMP,2.0)
        EDD2=RD1G*PFT*CTEMP*CMPLX(RVB1-RVB2,UVB1-UVB2)
        CTEMP=ED1+ED2+EDD1+EDD2
        ETDR(I)=REAL(CTEMP)
        ETDI(I)=AIMAG(CTEMP)
        WRITE (6,69) Y,ED1,ED2,EDD1,EDD2,CTEMP
  69    FORMAT (1H ,F9.4,10F10.6)
        Y=Y+DA
 100    CONTINUE
 200    CONTINUE
        YINC=DA
        A1=-A
        A2=-0.0001
        CALL ZINTG (EGR,EGI,A,A1,A2,YINC,NF,F,D)
        DO 610 I=1,NF
        WRITE (6,600) EGR(I),EGI(I)
```

```
600  FORMAT (5X,3HEG=,2E15.7)
610  CONTINUE
     A1=0.0001
     A2=1.0
     CALL ZINTG (ETPR,ETPI,A,A1,A2,YINC,NF,F,D)
     FNF=10.0
201  A1=A2
     A2=A1+1.0
     CALL ZINTG (BTPR,BTPI,A,A1,A2,YINC,NF,F,D)
     DO 210 N=1,NF
     ETPR(N)=ETPR(N)+BTPR(N)
     ETPI(N)=ETPI(N)+BTPI(N)
     WRITE (6,205) A2,BTPR(N),BTPI(N),ETPR(N),ETPI(N)
205  FORMAT (1H ,3HA2=,F10.4,5X,4HBTP=,2E15.7,5X,4HETP=,2E15.7)
210  CONTINUE
     IF (A1.LT.FNF) GO TO 201
     WRITE (6,300)
300  FORMAT (///6X,1HY,14X,8HE DIRECT,21X,11HE REFLECTED,21X,7HE TOTAL/
    2)
     Y=-A/2.0
     DO 310 I=1,NF
     CTEMP=CMPLX(ETDR(I)+ETPR(I),ETDI(I)+ETPI(I))
     WRITE (6,305) Y,ETDR(I),ETDI(I),ETPR(I),ETPI(I),CTEMP
305  FORMAT (1H ,F9.5,6E15.7)
     Y=Y+DA
310  CONTINUE
     DO 590 I=1,NF
     ETPR(I)=ETPR(I)+EGR(I)
     ETPI(I)=ETPI(I)+EGI(I)
590  CONTINUE
     WRITE (6,400)
400  FORMAT (///1H ,6X,1HY,15X,6HACTUAL,16X,22HEQUIVALENT LINE SOURCE/)
     Y=-A/2.0
     CTEMP1=CMPLX(ETDR(1)+ETPR(1),ETDI(1)+ETPI(1))
     DO 410 I=1,NF
     CTEMP2=CMPLX(ETDR(I)+ETPR(I),ETDI(I)+ETPI(I))
     EAM=CABS(CTEMP2)
     EAP=180.0/PI*ATAN2(AIMAG(CTEMP2),REAL(CTEMP2))
     RTE=SQRT(D**2+(Y+A/2.0)**2)
     CTEMP2=CTEMP1*SQRT(D/RTE)*CEXP(CMPLX(0.0,TPI*(D-RTE)))
     EQM=CABS(CTEMP2)
     EQP=180.0/PI*ATAN2(AIMAG(CTEMP2),REAL(CTEMP2))
     WRITE (6,405) Y,EAM,EAP,EQM,EQP
405  FORMAT (1H ,F9.4,4E15.7)
     Y=Y+DA
410  CONTINUE
     WRITE (6,700)
700  FORMAT (//5X,1HY,13X,21HTOTAL SCATTERED FIELD/)
     CTEMP=-CEXP(CMPLX(0.0,-TPI*(2.0*F+D)))
     Y=-A/2.0
     DO 710 I=1,NF
     CTEMP1=CTEMP+CMPLX(ETDR(I)+ETPR(I),ETDI(I)+ETPI(I))
     TEM1=CABS(CTEMP1)
     TEM2=180.0/PI*ATAN2(AIMAG(CTEMP1),REAL(CTEMP1))
     WRITE (6,705) Y,TEM1,TEM2
705  FORMAT (1H ,F9.5,5X,2E15.7)
     Y=Y+DA
710  CONTINUE
     WRITE (6,800)
800  FORMAT (///1H ,17HDIRECT DIFFRACTED//7X,1HY,15X,6HACTUAL,16X,22HEQ
    2UIVALENT LINE SOURCE/)
     Y=-A/2.0
     CTEMP1=CMPLX(ETDR(1),ETDI(1))
     DO 850 I=1,NF
```

```
      CTEMP2=CMPLX(ETDR(I),ETDI(I))
      EAM=CABS(CTEMP2)
      EAP=180.0/PI*ATAN2(AIMAG(CTEMP2),REAL(CTEMP2))
      RTE=SQRT(D**2+(Y+A/2.0)**2)
      CTEMP2=CTEMP1*SQRT(D/RTE)*CEXP(CMPLX(0.0,TPI*(D-RTE)))
      EQM=CABS(CTEMP2)
      EQP=180.0/PI*ATAN2(AIMAG(CTEMP2),REAL(CTEMP2))
      WRITE (6,405) Y,EAM,EAP,EQM,EQP
      Y=Y+DA
  850 CONTINUE
      CTEMP=CTEMP1*SQRT(D)*CEXP(CMPLX(0.0,TPI*D))
      WRITE (6,855) CTEMP
  855 FORMAT (50X,4HXA2=,2E15.7)
      WRITE (6,900)
  900 FORMAT (///1H ,50HREFLECTED DIFFRACTED PLUS GEOMETRICAL OPTICS STR
     2IP//7X,1HY,15X,6HACTUAL,16X,22HEQUIVALENT LINE SOURCE/)
      Y=-A/2.0
      CTEMP1=CMPLX(ETPR(1),ETPI(1))
      DO 950 I=1,NF
      CTEMP2=CMPLX(ETPR(I),ETPI(I))
      EAM=CABS(CTEMP2)
      EAP=180.0/PI*ATAN2(AIMAG(CTEMP2),REAL(CTEMP2))
      RTE=SQRT((D+2.0*F)**2+(Y+A/2.0)**2)
      CTEMP2=CTEMP1*SQRT((D+2.0*F)/RTE)*CEXP(CMPLX(0.0,TPI*(D+2.0*F-RTE)
     2))
      EQM=CABS(CTEMP2)
      EQP=180.0/PI*ATAN2(AIMAG(CTEMP2),REAL(CTEMP2))
      WRITE (6,405) Y,EAM,EAP,EQM,EQP
      Y=Y+DA
  950 CONTINUE
      CTEMP=CTEMP1*SQRT(D+2.0*F)*CEXP(CMPLX(0.0,TPI*(D+2.0*F)))
      WRITE (6,955) CTEMP
  955 FORMAT (50X,4HXA1=,2E15.7)
      TEMPA=A
      TEMPD=D
      GO TO 10
  500 CONTINUE
      STOP
      END
```

```
      SUBROUTINE ZINTG (ZINTGR,ZINTGU,A,A1,A2,YINC,NF,F,D)
      DIMENSION ZJR(100),ZJU(100),ZLR(100),ZLU(100),SR(100),SU(100),
     2ZJOR(100),ZJOU(100),ERRRE(100),ERRU(100),ZINTGR(100),ZINTGU(100),
     3FFAR(100),FFBR(100),FFAU(100),FFBU(100),FFQR(100),FFQU(100)
      CALL FNCTN (FFAR,FFAU,YINC,NF,A1,F,D,A)
      CALL FNCTN (FFBR,FFBU,YINC,NF,A2,F,D,A)
      DO 114 N=1,NF
      ZJR(N)=A2-A1
      ZJU(N)=0.0
      ZH=0.5*(A2-A1)
      ZLR(N)=ZH*(FFAR(N)+FFBR(N))
  114 ZLU(N)=ZH*(FFAU(N)+FFBU(N))
      NN=1
      DO 136 L=1,5
      DO 118 N=1,NF
      SR(N)=0.0
  118 SU(N)=0.0
      DO 124 I=1,NN
      FI=FLOAT(I)
      Q=(2.0*FI-1.0)*ZH+A1
      CALL FNCTN (FFQR,FFQU,YINC,NF,Q,F,D,A)
      DO 124 N=1,NF
      SR(N)=SR(N)+FFQR(N)
      SU(N)=SU(N)+FFQU(N)
  124 CONTINUE
      DO 132 N=1,NF
      ZJOR(N)=ZJR(N)
      ZJOU(N)=ZJU(N)
      ZJR(N)=ZLR(N)+4.0*ZH*SR(N)
      ZJU(N)=ZLU(N)+4.0*ZH*SU(N)
      ZLR(N)=(ZLR(N)+ZJR(N))/4.0
      ZLU(N)=(ZLU(N)+ZJU(N))/4.0
      ERRRE(N)=ABS((ZJR(N)-ZJOR(N))/ZJR(N))
      ERRU(N)=ABS((ZJU(N)-ZJOU(N))/ZJU(N))
  132 CONTINUE
      DO 133 N=1,NF
      IF (ERRRE(N).GT.1.0E-3) GO TO 135
      IF (ERRU(N).GT.1.0E-3) GO TO 135
  133 CONTINUE
      WRITE (6,20) L
   20 FORMAT (/3H L=,I2)
      GO TO 137
  135 NN=2*NN
      ZH=ZH/2.0
  136 CONTINUE
      WRITE (6,33) N,ERRRE(N),ERRU(N)
   33 FORMAT (1H ,2HN=,I5,5X,9HERRRE(N)=,E15.7,5X,8HERRU(N)=,E15.7)
  137 DO 138 N=1,NF
      ZINTGR(N)=ZJR(N)/3.0
  138 ZINTGU(N)=ZJU(N)/3.0
      RETURN
      END
```

```
      SUBROUTINE FNCTN (FFQR,FFQU,YINC,NF,YP,F,D,A)
      COMPLEX ED1P,EDD1P,CTEMP,ERDP,CTEMP1,CTEMP2
      DIMENSION FFQR(100),FFQU(100)
      PI=3.1415927
      TPI=2.0*PI
      IF (YP.LT.0.0) GO TO 100
      BETA=180.0/PI*ATAN2(YP,2.0*F)
      RHOP=SQRT(YP*YP+4.0*F*F)
      TEMP=BETA-180.0
      CALL VB (RVB1,UVB1,RHOP,TEMP,2.0)
      TEMP=BETA+180.0
      CALL VB (RVB2,UVB2,RHOP,TEMP,2.0)
      ED1P=-CMPLX(RVB1-RVB2,UVB1-UVB2)
      TEMP1=RHOP*A/(RHOP+A)
      CTEMP=-1.41421356*CMPLX(0.70710678,-0.70710678)/TPI*CEXP(CMPLX(0.0
     2,TPI*(TEMP1-RHOP-A)))/SQRT(RHOP+A)
      TEMP=270.0-BETA
      CALL VB (RVB1,UVB1,TEMP1,TEMP,2.0)
      TEMP=450.0-BETA
      CALL VB (RVB2,UVB2,TEMP1,TEMP,2.0)
      EDD1P=-CTEMP*CMPLX(RVB1-RVB2,UVB1-UVB2)
      ERDP=ED1P+EDD1P
      Y=-A/2.0
      DO 50 I=1,NF
      R1=SQRT(D*D+(Y-YP)*(Y-YP))
      R2=SQRT(D*D+(-Y-A-YP)*(-Y-A-YP))
      TEMP1=TPI*R1
      CALL HANKEL (BESL1,YNEU1,TEMP1)
      TEMP2=TPI*R2
      CALL HANKEL (BESL2,YNEU2,TEMP2)
      CTEMP=TPI*D/CMPLX(0.0,4.0)
      CTEMP1=CTEMP/R1*CMPLX(BESL1,-YNEU1)
      CTEMP2=CTEMP/R2*CMPLX(BESL2,-YNEU2)
      CTEMP=2.0*(CTEMP1+CTEMP2)*ERDP
      FFQR(I)=REAL(CTEMP)
      FFQU(I)=AIMAG(CTEMP)
      Y=Y+YINC
50    CONTINUE
      GO TO 200
100   CTEMP=CMPLX(0.0,-0.5)*CEXP(CMPLX(0.0,-TPI*2.0*F))
      Y=-A/2.0
      DO 150 I=1,NF
      R1=SQRT(D*D+(Y-YP)*(Y-YP))
      TEMP1=TPI*R1
      CALL HANKEL (BESL1,YNEU1,TEMP1)
      CTEMP1=TPI*D/R1*CTEMP*CMPLX(BESL1,-YNEU1)
      FFQR(I)=REAL(CTEMP1)
      FFQU(I)=AIMAG(CTEMP1)
      Y=Y+YINC
150   CONTINUE
200   CONTINUE
      RETURN
      END
```

```
C
C     J RICHMOND SUBROGRAM FOR FIRST ORDER CYLINDRICAL HANKEL FUNCTIONS
C
C     FROM SECTION 9.4 NBS HANDBOOK OF MATHEMATICAL FUNCTIONS PP 396 7
C
      SUBROUTINE HANKEL (BESL,YNEU,X)
      IF(X.GT.3.) GO TO 60
      R1=X/3.
      R2=R1*R1
      R4=R2*R2
      R6=R4*R2
      B1=X*(.5-.5624985*R2+.2109573*R4-.0395429*R6)
      Y1=    (-.6366198+.2212091*R2+2.1682709*R4-1.3164827*R6)/X
      IF(R1.LT.0.001) GO TO 55
      R8=R4*R4
      R10=R6*R4
      R12=R6*R6
      B1=B1+X*(.00443319*R8-.00031761*R10+.00001109*R12)
      Y1=Y1+(.3123951*R8-.0400976*R10+.0027873*R12)/X
 55   TEMP=2.0/3.1415927*ALOG(0.5*X)
      Y1=Y1+TEMP*B1
      GO TO 80
 60   CONTINUE
      IF (X.GT.200.0) GO TO 70
      R1=3./X
      R2=R1*R1
      R3=R1*R2
      R4=R2*R2
      R5=R3*R2
      R6=R3*R3
      SW=SQRT(X)
      F=.79788456+.00000156*R1+.01659667*R2+.00017105*R3
     2-.00249511*R4+.0011363*R5-.00020033*R6
      T=X-2.3561945+.12499612*R1+.0000565*R2-.00637879*R3+
     2.0007438*R4+.00079824*R5-.00029166*R6
      B1=F*COS(T)/SW
      Y1=F*SIN(T)/SW
      GO TO 80
 70   TEMP1=SQRT(2.0/3.1415927/X)
      TEMP2=X-3.0*3.1415927/4.0
      B1=TEMP1*COS(TEMP2)
      Y1=TEMP2*SIN(TEMP2)
 80   BESL=B1
      YNEU=Y1
      RETURN
      END
```

```
      SUBROUTINE VB (RVB,UVB,R,ANG,FN)
      COMPLEX DEM,TOP,COM,EXP,UPPI,UNPI
      DOUBLE PRECISION RAG,DP,TSIN
      PI=3.14159265
      TPI=6.28318530
      ANG=ANG*PI/180.0
      DEM=CMPLX(0.0,FN*SQRT(TPI))
      TOP=CEXP(CMPLX(0.0,-(TPI*R+PI/4.0)))
      COM=TOP/DEM
      N=IFIX((PI+ANG)/(2.0*FN*PI)+0.5)
      DN=FLOAT (N)
      A=1.0+COS(ANG-2.0*FN*PI*DN)
      BOTL=SQRT (TPI*R*A)
      EXP=CEXP(CMPLX(0.0,TPI*R*A))
      CALL FRNELS (C,S,BOTL)
      C=SQRT(PI/2.0)*(0.5-C)
      S= SQRT(PI/2.0)*(S-0.5)
      RAG=(PI+ANG)/(2.0*FN)
      TSIN=DSIN(RAG)
      TS=ABS(SNGL(TSIN))
      X=10.0
      Y=1.0/X**5
      IF(TS.GT.Y) GO TO 442
      COMP=-SQRT(2.0)*FN*SIN(ANG/2.0-FN*PI*DN)
      IF(COS(ANG/2.0-FN*PI*DN).LT.0.0) COMP=-COMP
      GO TO 443
  442 DP=SQRT(A)*DCOS(RAG)/TSIN
      COMP=SNGL(DP)
  443 UPPI=COM*EXP*COMP*CMPLX(C,S)
      N=IFIX((-PI+ANG)/(2.0*FN*PI)+0.5)
      DN=FLOAT(N)
      A=1.0+COS(ANG-2.0*FN*PI*DN)
      BOTL=SQRT(TPI*R*A)
      EXP=CEXP(CMPLX(0.0,TPI*R*A))
      CALL FRNELS (C,S,BOTL)
      C=SQRT(PI/2.0)*(0.5-C)
      S= SQRT(PI/2.0)*(S-0.5)
      RAG=(PI-ANG)/(2.0*FN)
      TSIN=DSIN(RAG)
      TS=ABS(SNGL(TSIN))
      IF(TS.GT.Y) GO TO 542
      COMP= SQRT(2.0)*FN*SIN(ANG/2.0-FN*PI*DN)
      IF(COS(ANG/2.0-FN*PI*DN).LT.0.0) COMP=-COMP
      GO TO 123
  542 DP=SQRT(A)*DCOS(RAG)/TSIN
      COMP=SNGL(DP)
  123 UNPI=COM*EXP*COMP*CMPLX(C,S)
      ANG=ANG*180.0/PI
      RVB=REAL (UPPI+UNPI)
      UVB=AIMAG(UPPI+UNPI)
      RETURN
      END
```

```
      SUBROUTINE FRNELS(C,S,XS)
      DIMENSION A(12),B(12),CC(12),D(12)
      A(1)=1.595769140
      A(2)=-0.000001702
      A(3)=-6.808568854
      A(4)=-0.000576361
      A(5)=6.920691902
      A(6)=-0.016898657
      A(7)=-3.050485660
      A(8)=-0.075752419
      A(9)=0.850663781
      A(10)=-0.025639041
      A(11)=-0.150230960
      A(12)=0.034404779
      B(1)=-0.000000033
      B(2)=4.255387524
      B(3)=-0.000092810
      B(4)=-7.780020400
      B(5)=-0.009520895
      B(6)=5.075161298
      B(7)=-0.138341947
      B(8)=-1.363729124
      B(9)=-0.403349276
      B(10)=0.702222016
      B(11)=-0.216195929
      B(12)=0.019547031
      CC(1)=0.0
      CC(2)=-0.024933975
      CC(3)=0.000003936
      CC(4)=0.005770956
      CC(5)=0.000689892
      CC(6)=-0.009497136
      CC(7)=0.011948809
      CC(8)=-0.006748873
      CC(9)=0.000246420
      CC(10)=0.002102967
      CC(11)=-0.001217930
      CC(12)=0.000233939
      D(1)=0.199471140
      D(2)=0.000000023
      D(3)=-0.009351341
      D(4)=0.000023006
      D(5)=0.004851466
      D(6)=0.001903218
      D(7)=-0.017122914
      D(8)=0.029064067
      D(9)=-0.027928955
      D(10)=0.016497308
      D(11)=-0.005598515
      D(12)=0.000838386
      IF(XS.LE.0.0) GO TO 414
      X=XS
      X=X*X
      FR=0.0
      FI=0.0
      K=13
      IF(X-4.0) 10,40,40
10    Y=X/4.0
20    K=K-1
      FR=(FR+A(K))*Y
      FI=(FI+B(K))*Y
      IF(K-2) 30,30,20
30    FR=FR+A(1)
      FI=FI+B(1)
```

```
      C=(FR*COS(X)+FI*SIN(X))*SQRT(Y)
      S=(FR*SIN(X)-FI*COS(X))*SQRT(Y)
      RETURN
40    Y=4.0/X
50    K=K-1
      FR=(FR+CC(K))*Y
      FI=(FI+D(K))*Y
      IF(K-2) 60,60,50
60    FR=FR+CC(1)
      FI=FI+D(1)
      C=0.5+(FR*COS(X)+FI*SIN(X))*SQRT(Y)
      S=0.5+(FR*SIN(X)-FI*COS(X))*SQRT(Y)
      RETURN
414   C=-0.0
      S=-0.0
      RETURN
      END
```

APPENDIX II

The Fortran IV computer program used in the computation of the reflection coefficient is as presented below.

```
$EXECUTE        PUFFT
$PUFFT    400
C       TE01 FLAP GUIDE REFLECTION COEFFICIENT
C       FREE SPACE REFLECTION COEFFICIENT NOT INCLUDED
        COMPLEX PFT,RD1,RDD1,RD1G,RT,XA1,XA2,C,CTEMP,CTP1,CTP2,CTP3
        DIMENSION VR(700),VI(700),GAMR(350),GAMI(350)
        PI=3.1415927
        TPI=2.0*PI
        PFT=CEXP(CMPLX(0.0,-PI/4.0))/TPI
        READ (5,9) A
 9      FORMAT (F10.4)
        WRITE (6,11) A
 11     FORMAT (30X,2HA=,F10.4////)
        A0R=ARSIN(0.5/A)
        A0=180.0*A0R/PI
        TEMP=1.0/COS((PI-A0R)/2.0)-1.0/COS((PI+A0R)/2.0)
        RD1=CMPLX(0.0,TEMP)
        TEMP=1.0/COS((1.5*PI-A0R)/2.0)-1.0/COS((1.5*PI+A0R)/2.0)
        RD1G=CMPLX(0.0,TEMP)
        CALL VB (RVB1,UVB1,A,90.0,2.0)
        CALL VB (RVB2,UVB2,A,270.0,2.0)
        RDD1=RD1G*CMPLX(RVB1-RVB2,UVB1-UVB2)
        RT=RD1+RDD1
        WRITE (6,10) RD1,RD1G,RDD1,RT
 10     FORMAT (///1H ,5H RD1=,2E15.7,5X,5HRD1G=,2E15.7/1X,5HRDD1=,2E15.7,
       27X,3HRT=,2E15.7////)
        C=RT*PFT/SQRT(TPI)/(2.0*A*COS(A0R))
        CTEMP=-RT/SQRT(TPI)*CEXP(CMPLX(0.0,-PI/2.0))
        VR(1)=REAL(CTEMP)
        VI(1)=AIMAG(CTEMP)
 100    READ (5,101) D,F,XA1,XA2,K
 101    FORMAT (6F10.6,I5)
        IF (K.EQ.0) GO TO 500
        WRITE (6,93) D,F,XA1,XA2
 93     FORMAT (//20X,2HD=,F10.4,10X,2HF=,F10.4/10X,4E15.7//)
        TD=2.0*D
        TDF=2.0*(D+F)
        CTP1=CEXP(CMPLX(0.0,-TPI*TD))/SQRT(TD)
        CTEMP=C*CTP1*CMPLX(VR(1),VI(1))
        GAMR(1)=REAL(CTEMP)
        GAMI(1)=AIMAG(CTEMP)
        GM=CABS(CTEMP)
        GP=180.0/PI*ATAN2(GAMI(1),GAMR(1))
        CTP2=CMPLX(VR(1),VI(1))*CTP1
        CTEMP=XA1*CTP2
        VR(2)=REAL(CTEMP)
        VI(2)=AIMAG(CTEMP)
        CTEMP=XA2*CTP2
        VR(3)=REAL(CTEMP)
        VI(3)=AIMAG(CTEMP)
        WRITE (6,150)
 150    FORMAT (1H ,6HBOUNCE,13X,13HMODAL VOLTAGE,17X,22HREFLECTION COEFFI
       2CIENT,9X,9HMAGNITUDE,3X,5HPHASE//)
        WRITE (6,151) VR(1),VI(1),GAMR(1),GAMI(1),GM,GP,VR(2),VI(2),VR(3),
       2VI(3)
 151    FORMAT (5X,1H1,5X,2E15.7,5X,2E15.7,5X,F10.6,F10.3/11X,2E15.7/11X,2
       2E15.7)
        DO 300 N=3,K
        CTP1=(0.0,0.0)
        CTP2=(0.0,0.0)
        K1=N-1
        DO 200 M=1,K1
        MD=2*M-1
        DUM=FLOAT(N-M-1)
```

```
      CTP1=CTP1+CMPLX(VR(MD),VI(MD))*CEXP(CMPLX(0.0,-TPI*(TD+DUM*TDF)))/
     2SQRT(TD+DUM*TDF)
  200 CONTINUE
      K2=N-2
      DO 220 M=1,K2
      MD=2*M
      DUM=FLOAT(N-M-1)
      CTP2=CTP2+CMPLX(VR(MD),VI(MD))*CEXP(CMPLX(0.0,-TPI*(DUM*TDF)))/SQR
     2T(DUM*TDF)
  220 CONTINUE
      CTP3=CTP1+CTP2
      CTEMP=C*CTP3
      ND=N-1
      GAMR(ND)=REAL(CTEMP)
      GAMI(ND)=AIMAG(CTEMP)
      GM=CABS(CTEMP)
      GP=180.0/PI*ATAN2(GAMI(ND),GAMR(ND))
      CTEMP=XA1*CTP3
      ND1=2*N-2
      VR(ND1)=REAL(CTEMP)
      VI(ND1)=AIMAG(CTEMP)
      CTEMP=XA2*CTP3
      ND2=2*N-1
      VR(ND2)=REAL(CTEMP)
      VI(ND2)=AIMAG(CTEMP)
      WRITE (6,250) ND,VR(ND1),VI(ND1),VR(ND2),VI(ND2),GAMR(ND),GAMI(ND)
     2,GM,GP
  250 FORMAT (1H ,I5,5X,2E15.7/11X,2E15.7,5X,2E15.7,5X,F10.6,F10.3)
  300 CONTINUE
      WRITE (6,350)
  350 FORMAT (////1H ,6HBOUNCE,5X,28HTOTAL REFLECTION COEFFICIENT,9X,9HM
     2AGNITUDE,8X,5HPHASE//)
      CTEMP=(0.0,0.0)
      K3=K-1
      DO 400 N=1,K3
      CTEMP=CTEMP+CMPLX(GAMR(N),GAMI(N))
      GM=CABS(CTEMP)
      GP=180.0/PI*ATAN2(AIMAG(CTEMP),REAL(CTEMP))
      WRITE (6,360) N,CTEMP,GM,GP
  360 FORMAT (1H ,I5,5X,2E15.7,5X,2E15.7)
  400 CONTINUE
      GO TO 100
  500 CONTINUE
      STOP
      END
```